

Impact of Strain on the Performance of InGaN-based Multijunction Solar Cell

by

Md. Aminur Rahman

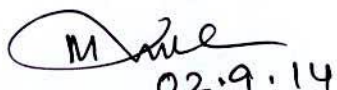
A thesis submitted in partial fulfillment of the requirements for the degree of
Master of Science in Electrical and Electronic Engineering




Khulna University of Engineering & Technology
Khulna-920300, Bangladesh
September 2014

Declaration

This is to certify that the thesis work entitled "*Impact of Strain on the Performance of InGaN-based Multijunction Solar Cell*" has been carried out by *Md. Aminur Rahman* in the Department of *Electrical and Electronic Engineering*, Khulna University of Engineering & Technology, Khulna, Bangladesh. The above thesis work or any part of this work has not been submitted anywhere for the award of any degree or diploma.


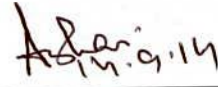
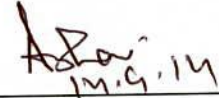
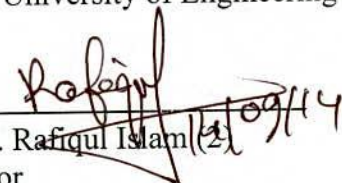
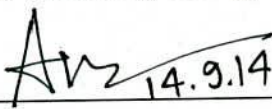

02.9.14
Signature of Supervisor


02.09.14
Signature of Candidate

Approval

This is to certify that the thesis work submitted by *Md. Aminur Rahman* entitled " *Impact of Strain on the Performance of InGaN-based Multijunction Solar Cell* " has been approved by the board of examiners for the partial fulfillment of the requirements for the degree of *Master of Science in Electrical and Electronic Engineering* in the Department of *Electrical and Electronic Engineering*, *Khulna University of Engineering & Technology*, *Khulna, Bangladesh* in *September 2014*.

BOARD OF EXAMINERS

- | | | |
|----|--|--------------------------|
| 1. | 
14.9.14
<hr style="width: 80%; margin-left: 0;"/> Dr. Md. Rafiqul Islam (1)
Professor
Department of Electrical and Electronic Engineering
Khulna University of Engineering & Technology | Chairman
(Supervisor) |
| 2. | 
<hr style="width: 80%; margin-left: 0;"/> Head
Department of Electrical and Electronic Engineering
Khulna University of Engineering & Technology | Member |
| 3. | 
<hr style="width: 80%; margin-left: 0;"/> Dr. Ashraful G. Bhuiyan
Professor
Department of Electrical and Electronic Engineering
Khulna University of Engineering & Technology | Member |
| 4. | 
<hr style="width: 80%; margin-left: 0;"/> Dr. Md. Rafiqul Islam (2)
Professor
Department of Electrical and Electronic Engineering
Khulna University of Engineering & Technology | Member |
| 5. | 
<hr style="width: 80%; margin-left: 0;"/> Dr. Md. Anwarul Abedin
Professor
Department of Electrical and Electronic Engineering
Dhaka University of Engineering & Technology, Gazipur | Member
(External) |

Acknowledgement

It is a great pleasure for me to express unbound indebted gratitude to my supervisor Dr. Md. Rafiqul Islam (1), Professor, Department of Electrical and Electronic Engineering of Khulna University of Engineering & Technology, for his numerous helpful and constructive suggestions, scholastic guidance, constant inspiration and support, valuable advice and kind cooperation for the successful completion of the thesis work. He has always been extremely generous with his time, knowledge and ideas, and allowed me great freedom for the completion of the research. His enthusiastic approach to research, his endless excitement in multi-physics, solar cell, especially strain-issues in semiconductor materials and devices and his effervescent personality have made this thesis all the more enjoyable and I am greatly encouraged.

I am highly grateful to Dr. Md. Rafiqul Islam (2), Professor, Department of Electrical and Electronic Engineering, Khulna University of Engineering & Technology who was the pioneer and inspiring person to me. His valuable advice, morality, support and enthusiastic encourage always finds path for me. My cordial thanks is also extended to Md. Jahirul Islam, Assistant Professor, Dept. of EEE, KUET, for giving many ideas and for his in-depth knowledge in the field of semiconductor material and multi-junction solar cell. His helpful discussion about physical properties of semiconductor material made my research easy.

I would like to thank to the ex-students of EEE Dept., KUET, Md. Imran Hasan, Md. Mottaleb Hossain Liton, and Md. Moshir Rahman for their encouragement. Many times, they helped me to collect information and ideas related to this research work.

I would also like to thank my family and friends for their encouragement and moral support.

Author

Abstract

Strain issue and its impact on the performance of InGaN-based multijunction solar cell (MJSC) is addressed for the first time in the present research work. The route of strain in MJSC is identified to be due to the change in lattice constants in different layers of subcell grown epitaxially with bandgap stepping. Using multi-layered strain model, the state of strain and its magnitude is determined for three kinds of MJSC structures named as MJSC-1, MJSC-2 and MJSC-3. The results are expressed in terms of subcell thickness 80nm, 100nm and 120nm and number of subcells 3, 5 and 7. It is found that the magnitude of MJSC position-dependent strain is strongly dependent on the subcell thickness and decreases with increasing the layer thickness. Further, the position-dependent strain increases with increasing the number of subcells. With the combination of MJSC position-dependent strain and deformation potentials, the strain-induced energy bandgap modification is determined under tensile strain condition. Finally, including the strain effect the efficiencies of different MJSC structures are evaluated and found to be lower with that of reported without taking into account of strain. The detraction of efficiency is identified to be due to the open circuit voltage which decreases under tensile strain condition. Among the MJSC structures studied here, MJSC-3 with 7-layers is less efficient and its efficiency decreases upto 3.01% when strain effect is taken into consideration.

Contents

		PAGE
	Title Page	i
	Declaration	ii
	Certificate of Research	iii
	Acknowledgement	iv
	Abstract	v
	Contents	vi
	List of Tables	viii
	List of Figures	ix
	List of Symbol	xii
CHAPTER I	Introduction	1
	1.1 General Information	1
	1.2 Historical Background	2
	1.3 Related Works	3
	1.4 Objectives of the Research Work	6
	1.5 Layout of The Thesis	7
CHAPTER II	Solar Cell Fundamentals	9
	2.1 Introduction	9
	2.2 Band Theory	10
	2.3 Physical Representation of a Solar Cell	12
	2.4 Working Principle of Solar Cell	14
	2.5 Efficiency loss Factors in Solar Cell	16
	2.5.1 Reflection Loss	17
	2.5.2 Recombination Loss	17
	2.5.3 Series and Shunt Resistance Loss	18
	2.5.4 Inadequate Absorption of Photons	18
	2.5.5 Thermal Loss	18
	2.5.6 Inadequate Assortment of EHPs	19
	2.5.7 Fill Factor (FF) Loss	19
	2.6 Efficiency Enhancement Technique	20
	2.6.1 MJ solar Cell	21
	2.6.2 Multiple Spectrum Solar Cell	21
	2.6.3 Compound Absorption Path Solar Cell	22
	2.6.4 Multiple Energy Level Solar Cell	23
	2.6.5 Multiple Temperature Solar Cell	24
	2.7 Important Fabrication Issues in MJSC	24

	2.7.1 Bandgap Issue	25
	2.7.2 Lattice Mismatch Issue	25
	2.7.2.1 Energy Bandgap under the Influence of Strain	26
	2.7.3 Current Matching Issue	27
	2.7.4 Use of Tunnel Junction	28
	2.8 Typical MJSC Models	28
	2.9 Existence of Strain in Multilayer Structure	30
CHAPTER III	Multijunction Solar Cell Structure and Strain Model	32
	3.1 Introduction	32
	3.2 Properties of $\text{In}_x\text{Ga}_{1-x}\text{N}$	33
	3.2.1 Band Gap Energy	33
	3.2.2 Absorption Coefficient α	34
	3.2.3 List of Important Parameters	35
	3.3 InGaN-based MJSC Structures	36
	3.4 Multi-layered Strain Model	37
	3.5 Strain-Induced Change in Energy Bandgap	40
	3.6 Photo-current Density	40
	3.7 Strain Effect on Open Circuit Voltage	42
	3.8 Efficiency	43
CHAPTER IV	Performance of MJSC in Presence of Strain	44
	4.1 Introduction	44
	4.2 Analysis of Strain in Different MJSC structures	44
	4.2.1 MJSC Structure Dependent Strain	45
	4.2.2 Subcell Layer Dependent Strain	48
	4.2.3 Subcell Thickness Dependent Strain	50
	4.2.4 Effect of strain on the change in subcell thickness	52
	4.2.5 Strain induced change in energy gap	54
	4.2.6 The change in energy gap due to subcell thickness dependent strain	57
	5.3 Performance of MJSCs in presence of strain	59
CHAPTER V	Conclusion and Future Work	63
	5.1 Conclusion	63
	5.2 Proposal for Future Works	64
References		65

LIST OF TABLES

Table No.	Description	Page
3.1	Bandgap energy distribution of different subcells of MJSC	34
3.2	Properties of GaN and InN materials [46-49]	36
4.1	Values of subcell position dependent strain with respect to subcell thickness 80 nm, 100 nm and 120 nm for different MJSC structures.	45
4.2	Comparison of subcell position-dependent strain with respect to the number of subcell layers and thicknesses of MJSC-1	48
4.3	Comparison of cell position-dependent strains estimated for the subcell thickness of 80nm, 100nm and 120nm when subcell numbers are 3 (a) MJSC-1, (b) MJSC-2, and (c) MJSC-3	50
4.4	Change in strain, $\Delta\varepsilon$, due to differential change in subcell thickness from 120 to 100nm and from 120 to 80nm	52
4.5	Comparison of relaxed and strained bandgap energies under tensile strain. The results are estimated for different MJSCs having 3, 5 and 7 layers	55
4.6	Comparison of subcell thickness dependent strain induced change in energy gap, ΔE_{gs} , for different thicknesses of the subcells. The comparison is made for 3, 5 and 7 layers of MJSC-3	57
4.7	Comparison of ΔE_{gs} for different MJSCs with 3, 5 and 7 layers	58
4.8	Comparison of the open circuit voltage, V_{oc} , short circuit current, I_{sc} , average number of photons and efficiency, η , for different MJSC structures with and without strain effects.	60

LIST OF FIGURES

Figure No.	Description	Page
1.1	Multijunction Solar Cell Roadmap [16].	4
1.2	Band gap energies of the $\text{In}_x\text{G}_{1-x}\text{N}$ alloy system cover the entire air-mass-1.5 solar spectrum. The band gap energies of conventional MJ solar cell materials (Ge, GaAs and GaInP) are also shown in the right hand panel for comparison [20]	5
2.1	Comparison of Band Gaps for Different Material Types [30]	11
2.2	Comparison of single junction-Si solar cell to common triple junction solar cell [31]	11
2.3	Solar irradiance absorption comparison of single junction-Si solar cell to common triple junction solar cell [32]	12
2.4	Schematic of a typical solar cell [33]	13
2.5	The working principle of solar cell.	15
2.6	Solar cell operation.	16
2.7	Current- voltage characteristics of a solar cell.	20
2.8	Multiple spectrum photovoltaic system	22
2.9	Absorption in compound absorption path solar cell	22
2.10	Operation of multiple energy level solar cells as (a) quantum well solar cell & (b) intermediate band solar cell.	23
2.11	Concept of multiple temperatures solar cells	24
2.12	Relationship between bandgap energies and lattice constants of the semiconductors.	26
2.13	Absorption coefficient versus wavelength for various semiconductor materials [42].	27
2.14	Current density–Voltage (J–V) characteristic of a tunnel junction	28
2.15	(a) Multijunction principle representation. (b) InGaP-based Multijunction Solar Cell.	29
2.16	(a) Individual subcell with different composition, corresponding lattice constant (b) Multilayer Structure having different subcell bandgap energies	30

3.1	Compositional dependence of band gap energy of InGaN material.	34
3.2	Room temperature absorption coefficient of $\text{In}_x\text{Ga}_{1-x}\text{N}$ alloys as a function of photon energy with different indium composition, x [45].	35
3.3	The schematic illustration of (a) MJSC-1, (b) MJSC-2 and (c) MJSC-3 [22-24].	37
3.4	Multilayer structure with n-layer	38
3.5	Solar energy spectrum (AM of 1.5) in terms of photon vs. photon energy [52]	41
4.1	Comparison of cell position-dependent strains estimated for the MJSC-1, MJSC-2 and 3 when subcell numbers are 3 (a) 80 nm thick subcell (b) 100 nm thick subcell, and (c) 120 nm thick subcell	46
4.2	Comparison of cell position-dependent strains estimated for the MJSC-1, MJSC-2, and MJSC-3 when subcell numbers are 5 (a) 80 nm thick subcell (b) 100 nm thick subcell, and (c) 120 nm thick subcell	46
4.3	Comparison of cell position-dependent strains estimated for the MJSC structures 1, 2, and 3 when the subcell numbers are 7 (a) 80 nm thick subcell (b) 100 nm thick subcell, and (c) 120 nm thick subcell	47
4.4	Comparison of cell position-dependent strains estimated for the number of subcell 3, 5 and 7 of the MJSC-1 (a) 80 nm thick subcell (b) 100 nm thick subcell, and (c) 120 nm thick subcell.	48
4.5	Comparison of cell position-dependent strains estimated for the number of subcell 3, 5 and 7 subcell of the MJSC-2 (a) 80 nm thick subcell (b) 100 nm thick subcell, and (c) 120 nm thick subcell.	49
4.6	Comparison of cell position-dependent strains estimated for the number of subcell 3, 5 and 7 subcell layered structure of MJSC-3 (a) 80 nm thick subcell (b) 100 nm thick subcell, and (c) 120 nm thick subcell	49
4.7	Comparison of cell position-dependent strains estimated for the subcell thicknesses of 80nm, 100nm and 120nm when subcell numbers are 3 (a) MJSC-1, (b) MJSC-2, and (c) MJSC-3	51
4.8	Comparison of cell position-dependent strains estimated for the subcell thickness of 80nm, 100nm and 120nm when subcell numbers are 5 (a) MJSC-1, (b) MJSC-2, and (c) MJSC-3	51

4.9	Comparison of cell position-dependent strains estimated for the subcell thickness of 80nm, 100nm and 120nm when subcell numbers are 7 (a) MJSC-1, (b) MJSC-2, and (c) MJSC-3	52
4.10	Change in cell position-dependent strains, $\Delta\varepsilon$ due to the differential change in subcell thickness of Δt (120nm-80nm) and Δt (120nm-100nm) when subcell numbers are 3 (a) MJSC-1, (b) MJSC-2 and (c) MJSC-3	53
4.11	Change in cell position-dependent strains, $\Delta\varepsilon$ due to the differential change in subcell thickness of Δt (120nm-80nm) and Δt (120nm-100nm) when subcell numbers are 5 (a) MJSC-1, (b) MJSC-2 and (c) for MJSC-3	53
4.12	Change in cell position-dependent strains, $\Delta\varepsilon$ due to the differential change in subcell thickness of Δt (120nm-80nm) and Δt (120nm-100nm) when subcell numbers are 7 (a) MJSC-1, (b) MJSC-2 and (c) MJSC-3	54
4.13	Comparison of unstrained and strained bandgap energies for MJSC-1 (a) 3-layer (b) 5-layer and (c) 7-layer with subcell thickness 80nm. The bandgap energies are estimated under tensile strained condition.	55
4.14	Comparison of unstrained and strained bandgap energies for MJSC-2 (a) 3-layer (b) 5-layer and (c) 7-layer with subcell thickness 80nm. The bandgap energies are estimated under tensile strained condition.	56
4.15	Comparison of unstrained and strained bandgap energies for MJSC-3 (a) 3-layer (b) 5-layer and (c) 7-layer with subcell thickness 80nm. The bandgap energies are estimated under tensile strained condition.	56
4.16	Comparison of strain-induced change in energy gap, ΔE_{gs} , for the subcell thicknesses 80nm, 100nm and 120nm. The results are estimated for MJSC-3 when the number of subcells are (a) Three (b) Five and (c) Seven.	58
4.17	Comparison of strain-induced change in energy gap for MJSC-1, 2 and 3 structures when the number of subcells are (a) Three (b) Five and (c) Seven and the cell thickness is taken as 80 nm.	59
4.18	Comparison of efficiencies for different MJSCs under strained and unstrained conditions	61

List of Symbols

α	Absorption coefficient
η	Efficiency of solar cell
ϕ_0	Incident irradiance per unit area (mW/cm^2)
ϵ	Di-electric constant
BSF	Back surface field
D_p	Drift velocity of hole
D_n	Drift velocity of electron
EHP	Electron-hole pair
E_g	Band gap energy
E_0	Built-in-field
FF	Fill Factor
F	No. of incident photon
H'	Thickness of p-region
I_{mp}	Current in maximum power condition
I_{SC}	Short circuit current
J_{SC}, J_L	Short circuit current density
J_0	Saturation current density
J_{ph}	Photogenerated current
J_n	Photogenerated current in n-region

J_p	Photogenerated current in p-region
L_n	Diffusion length of electron
l_n	Length of neutral n-region
L_p	Diffusion length of hole
l_p	Length of neutral p-region
N_A	Acceptor atom concentration
N_D	Donor atom concentration
N_C	Density of state for conduction band
N_V	Density of state for valance band
n_i	Intrinsic carrier concentration
R	Reflection co-efficient
S_n	Surface recombination velocity in n-region
S_p	Surface recombination velocity in p-region
SCL	Space charge layer
T	Temperature
V_{OC}	Open circuit voltage
V_{mp}	Voltage in maximum power condition
W	Depletion width
X_j	Thickness of n-region
x	Indium composition in $\text{In}_x\text{Ga}_{1-x}\text{N}$
MJ	Multi-Junction

MJSC	Multi-Junction Solar Cell
ρ	Poisson's ratio
a	Lattice constant
E	Young's modulus
$C_{11}, C_{12}, C_{13}, C_{33}$	Elastic constants (GPa)
D'_1, D'_2, D'_3, D_4	Deformation potentials (eV)
K	Uniform strain component
y	MJSC position
y_b	y-level where bending strain is zero
G	Radius of curvature
t	Subcell thickness
ϵ_i^0	Initial strain
ΔE_{gs}	Strain-induced change in band gap energy
J_{dr}	Current density in depletion region
E_{gs}	Band gap energy under strain condition
AM	Air Mass

CHAPTER I

Introduction

1.1 General Information

Nowadays development of modern civilization and industries are highly dependent on electrical power. Generation of electrical power from conventional resources (such as coal, gas, and oil) produces greenhouse gases as a byproduct, which is in fact responsible for global warming/changing our environment [1]. Some of these resources are only available in few regions of the world; the scarcity also poses a risk to national and regional infrastructures. The fossil fuel is costly for transmitting in remote areas. On the other hand, the use of nuclear and chemical energy is a questionable solution due to its radioactive disposal and toxic waste. Therefore, the needs of renewable energy resources are considered very important to meet up the world energy demand and to defend the environment from climate change phenomenon due to the burning of fossil fuels. The renewable energy resources such as wind, hydro, biomass and solar energies have the prospective to overcome the above problems [2]. The sunlight is an unlimited environmental pollution free clean source of renewable energy. Solar cell is an optoelectronic device that can convert light energy into electrical energy [3]. It can provide electrical power at low operating cost and is virtually free from environmental pollution. Bangladesh is situated closer to the equilateral zone and here solar energy is available throughout the year with a good potential. Also we have a significant amount of remote areas especially the coastal zone where it is very difficult

to erect transmission lines or gas pipes. That's why solar system may be deployed in these areas to meet up the electrical energy demand of the people living there.

1.2 Historical Background

In the year 1767 a Swiss scientist named Horace-Benedict de Saussure created the first solar collector – an insulated box covered with three layers of glass to absorb heat energy [4]. Saussure's box became widely known as the first solar oven, reaching temperatures of 230 degrees Fahrenheit. A French scientist by the name Edmond Becquerel discovered a major milestone in the evolution of solar energy at 1839 [5]. He defines the photovoltaic effect using two electrodes placed in an electrolyte, when sunlight exposes into the junction, electricity is produced. Some years later, in 1876, English scientist Grylls Adams discovered that if pieces of the metals selenium and platinum touched each other, and light shone on them, electricity started to flow through the metals-called photovoltaic effect. Solar cell was invented around 1886 by the American Charles Fritts [6]. It was made with the metal selenium coated with a layer of gold which was very costly, inefficient, and transforming less than 1 percent of the absorbed light into electrical energy. Substantial improvements in solar cell efficiency had been achieved for a better understanding of the physical principles involved in their design, provided by Einstein in 1905 and Schottky in 1930 [7]. By the 1930s both the selenium cell and copper oxide cell were being employed in light sensitive devices such as photometers to use in photography. Solar cell efficiency finally saw generous progress with the development of first silicon cell by Russell Ohl. in 1941. In 1953, Calvin Fuller, Gerald Pearson, and Daryl Chapin, discovered the silicon solar cell capable of 6% energy conversion efficiency. However in the 1970's, Exxon Corporation designed an efficient solar panel which was less costly to manufacture. This was a major milestone in the history of solar energy. In 1980, the silicon cells as well as the cells made of gallium

arsenide, with more than 20 percent efficiencies were fabricated. In 1889 a concentrator solar cell in which sunlight is concentrated onto the cell surface by means of lenses, achieved an efficiency of 37%. By the year 1999 the largest plant was developed producing more than 20 kilowatts. With the solar victory, in 2012, the history's largest solar energy plant is the Golmud Solar Park in China, with an installed capacity of 200 megawatts [8]. However, still the efficiency of conventional and commercially available solar cells is poor. Other associative drawbacks, such as optimum power controlling and tracking of PV array have been solved within the present technology.

Researchers are now concentrating their investigation to achieve higher efficiency in solar cell technology. The modifications of design and fabrication technology with the coordination of different materials are being carried out to reduce the reflected component of solar energy. It is evident from the literatures of this field that there are a lot of materials available on low cost and high efficiency solar cells with improved performance. Single junction solar cell is not able to utilize full spectrum of solar energy to electrical energy. The photons of higher energy than the semiconductor bandgap energy is usually dissipated as heat and is thus wasted. On the other hand, photons of lower energy than bandgap are not absorbed at all and hence unused. To overcome these difficulties and hence to increase the solar cells efficiency multijunction(MJ) approach has been used all over the world [9].

1.3 Related Works

To be competitive with the conventional energy resources, the conversion efficiency of a solar cell must be improved. In previous studies [10, 11], several solar cell approaches have been proposed like multijunction (MJ) solar cell, concentrator solar cell, intermediate bandgap solar cell, quantum well, quantum dot solar cells etc. Among them MJ approach is very much attractive to resolve the main issues related with efficiency degradation.

To utilize the whole solar spectrum MJSC are fabricated with the combination of different bandgap materials or by selecting suitable composition in ternary/quaternary materials, subcells with different bandgaps are formed. Bedair *et al.* [12] demonstrated the first multijunction solar cell with epitaxially grown subcells monolithically interconnected with an epitaxially grown tunnel junction with an AlGaAs/GaAs two-junction cell in 1979. Several years later, Olsen *et al.* [13] demonstrated the dual junction GaInP/GaAs cell, and this technology was deployed on space missions in the mid-1990. An active Ge bottom subcell was developed, using the Ge substrate, resulting in three-junction (3J) GaInP/GaInAs/Ge cells which were first launched on spacecraft in 2000. In 2006, 40% efficiency was achieved for 3J- GaInP/GaInAs/Ge cells [14]. A 3J lattice-matched cell with an undisclosed lattice matched technology has achieved 43.5% efficiency [15]. Spectrolab has a broad research program pursuing a variety of development paths toward improved efficiency as shown in figure 1.1.

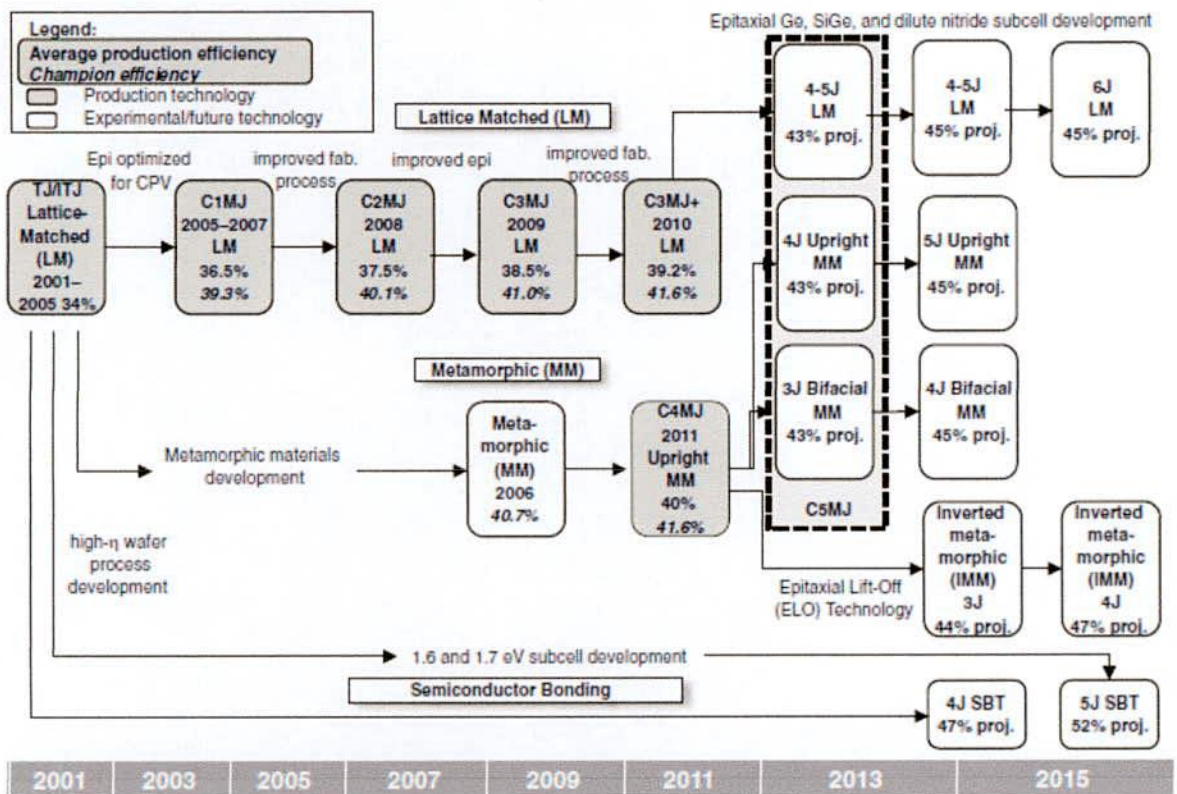


Figure 1.1: Multijunction Solar Cell Roadmap [16].

On the other hand a tri-valent composition InGaP/GaAs cell has the highest efficiency of 30.3% under AM1.5G solar spectrum with 1-sun intensity (100 mW cm^{-2}) among monolithic 2J cells [17, 18], while 4-terminal configuration allowed the highest 2J efficiency of 32.6% under AM1.5G spectrum at 100 suns for a lattice-mismatched GaAs/GaSb stack (GaSb: 6.09 \AA , 0.70 eV) [19].

It is well recognized that $\text{In}_x\text{Ga}_{1-x}\text{N}$ (0.64 to 3.4 eV) is a promising material [21] for multijunction solar cell (MJSC), because its bandgap energy is nicely matched to whole solar spectrum as indicated in figure 1.2. The InGaN-based MJSC structure is composed of number of subcells in which the bandgaps of the subcells are divided by tuning the composition. For efficient absorption of whole solar energies, the higher bandgap cell is fabricated at the top and others are below the top cell.

In case of MJSC structure, cells are fabricated layer by layer resulting in layered change in lattice constant. Since the lower bandgap cell is placed at the bottom and higher at the top of InGaN-based MJSC structure, the lattice constant decreases in different layers from bottom to

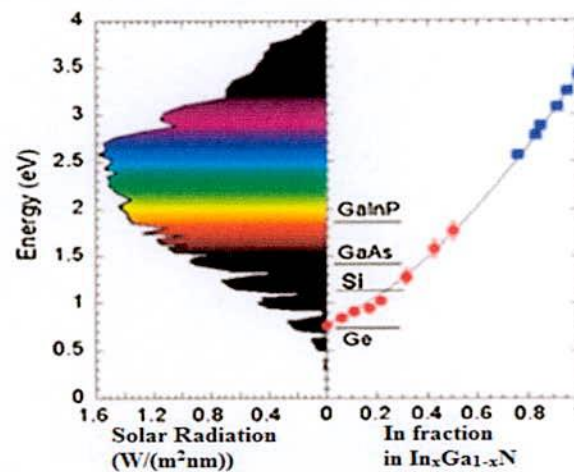


Figure 1.2: Band gap energies of the $\text{In}_x\text{Ga}_{1-x}\text{N}$ alloy system cover the entire air-mass-1.5 solar spectrum. The band gap energies of conventional MJ solar cell materials (Ge, GaAs and GaInP) are also shown in the right hand panel for comparison [20].

top that leads to induce tensile strain and cannot be determined using simple epilayer strain model. In order to determine strain from the MJSC structure multilayered strain model can be used where strain is calculated by integrating strain induced in different layers due to change in lattice constant layer by layer. In previous studies [21-23], efficiencies of MJSC structures are reported without considering strain effect. To understand the true efficiency of MJSC it is very much important to evaluate the efficiency taking into account of strain effect, which has not been done yet.

1.4 Objectives of the Research Work

In previous studies [23, 24] the efficiency of InGaN-based MJSC was investigated without taking into account of strain. It is well known that the bandgap of semiconductor materials is modified under the influence of strain. Due to the application of compressive strain the bandgap of InGaN is increased and opposite is happened for the tensile strain [25]. It is therefore very much important to explore the actual efficiency of InGaN-based MJSC on account of strain.

It is well established that the lattice mismatch between GaN ($a_{\text{GaN}}=3.189 \text{ \AA}$) and InN ($a_{\text{InN}}=3.54 \text{ \AA}$) is more than 10% [26]. Epitaxially fabricated different subcell layers will therefore induce as well as the strain model in MJSC structure and cannot be determined using simple epilayer strain model [22] or the strain model used to determine strain in bulk materials [27].

In this work, study of strain will be carried out in different MJSC structures using multilayered strain model [28-29]. Three types of MJSC structures [22-24] will be considered in the present study. The state of strains and their magnitudes will be investigated as a function of cell parameters. The strains will also be studied with respect to the number of

layers for different MJSC structures. With the combination of multilayered strain model and electron deformation potentials, the strain-induced change in bandgap energy, ΔE_{gs} will be estimated. The resultant open circuit voltage of subcells is then determined from the summation of ΔE_{gs} and the relaxed bandgap, E_g under tensile strained condition. Finally, the efficiency of different MJSC structures will be calculated including the effect of strain in terms of number of subcells and their thicknesses.

1.5 Layout of The Thesis

This dissertation describes the impact of strain on the performance of InGaN-based multijunction solar cell. The research work is divided into several chapters in which solar cell fundamentals, solar cell structures, mathematical modelling of strain, strain-dependent bandgap energy calculation and performances are discussed.

In chapter 1, background of the present work is explained. Present status and future prospect of InGaN-based MJSC are described clearly in this chapter. Finally objectives of the present work are also summarized in this chapter.

In chapter 2, the working principle and issues related to efficiency losses of solar cell are discussed. The efficiency enhancement techniques and the influence of strain on the performance improvement of photovoltaics using MJ method have also been discussed in this chapter.

Chapter 3 starts with a description of physical and electronic properties of InGaN material. The potentiality of InGaN material for MJSC fabrication is explained here. Three MJSC structures with the distribution bandgap energy in different subcells are presented in this chapter. The mathematical modelling of the proposed device has been presented. The origin

of strain in MJSC structure has been discussed along with multilayer strain model. The strain-induced modification of energy bands in InGaN semiconductor has also been discussed. Furthermore, the mathematical formulations associated with solar cell efficiency in presence of strain have been explained.

In chapter 4, the performance of different MJSC structures is determined using the formulations discussed in chapter 3 and the results obtained for different MJSC structures with and without strain effect are summarized. Finally, a comparison is made among the MJSC structures to understand the better performance of the MJSC structures with and without taking into account of strain.

Chapter 5 provides the conclusion of the present research and the prospect for the future studies.

CHAPTER II

Solar Cell Fundamentals

2.1 Introduction

Solar electricity or photovoltaics can meet up the substantial portion of electrical power demand without burning fossil fuels (coal, oil or natural gas) or creating nuclear fission reactions. The sun provides us with an unlimited amount of pollution free, environmentally friendly, reliable energy. Photovoltaics can generate electricity for a wide range of applications. It is a cost-effective way to provide power to remote areas and for space applications. However, the most important drawback of solar energy converter (solar cell) is its lower conversion efficiency. Better efficiencies are needed if solar technology is to become a larger contender in the movement toward alternative energy sources. Such mandate increases in efficiency has been expected in a class of PV known as multijunction solar cells. The main principle being the use of multiple semiconductors arranged in a stack to more effectively capture electromagnetic radiation than the standard single junction cells. Current records in multijunction solar cell efficiencies are over 40% and show the promise for values above 50% in the coming years. Multijunctions are arguably the most promising area of PV technologies and are critical in the development of a green energy infrastructure. Attempts have been made to fabricate photovoltaic cells with materials other than silicon. At the same time modification in design are being carried out to reduce the reflected component of solar

energy. The modelling and hence to investigate the performance of $\text{In}_x\text{Ga}_{1-x}\text{N}$ -based MJSC is very much promising for its wide range of composition dependent bandgap (0.64 to 3.4 eV) properties. In this chapter, the working principle and efficiency losses of solar cell have been discussed. The efficiency enhancement techniques and the influence of strain on the performance improvement of photovoltaics using MJ method have also been discussed in this chapter.

2.2 Band Theory

A brief discussion of band theory is required before the evaluation and an ultimate understanding of solar cells principles. The classical Bohr model of the atom is insufficient when analyzing semiconductors, so a better model is needed; this leads to Band Theory. In Band Theory there are three classifications of material: insulator, semiconductor, and conductor. The difference between each material is the size of the energy needed to move from one energy state or “band” to another. This difference in energy is called the “energy band gap” or simply “band gap”. The smaller the band gap, the better a material is able to conduct the flow of charge carriers (i.e. electrons) from energy state to energy state giving rise to electric current. The lower energy band is referred to as the valence band and the upper energy band is referred to as the conduction band [30].

According to natural processes carriers want to minimize their energy. For this reason, carriers are found in mass quantity in the valence band and in small amounts in the conduction band during thermal equilibrium conditions, thus many high energy states are available to carriers, but these states are mostly empty because the carriers do not have enough energy to move from a low energy to a high energy state under normal thermal equilibrium situations. As shown in figure 2.1, insulators have a large band gap and the band gap of conductors is thought to be zero [30].

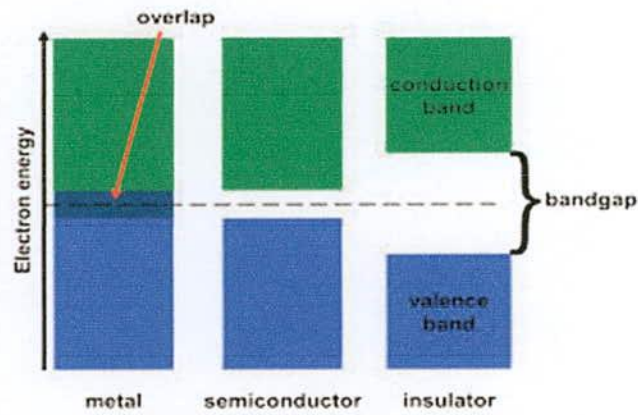


Figure 2.1: Comparison of Band Gaps for Different Material Types [30].

A great level of control may be attained by controlling the ability to have a material conduct at will. Such a level of control is available in semiconductors because the band gaps are small enough such that natural and easily attainable man-made processes can provide enough energy to charge carriers to traverse the band gap, going from the lower energy state in the valence band to the higher energy state in the conduction band. When considering solar cells, the band gaps in the semiconductors used need to be comparable to the energy of incoming photons. Figure 2.2 provides a graphical example of the band gaps and relationship to common parts of the electromagnetic Spectrum [31].

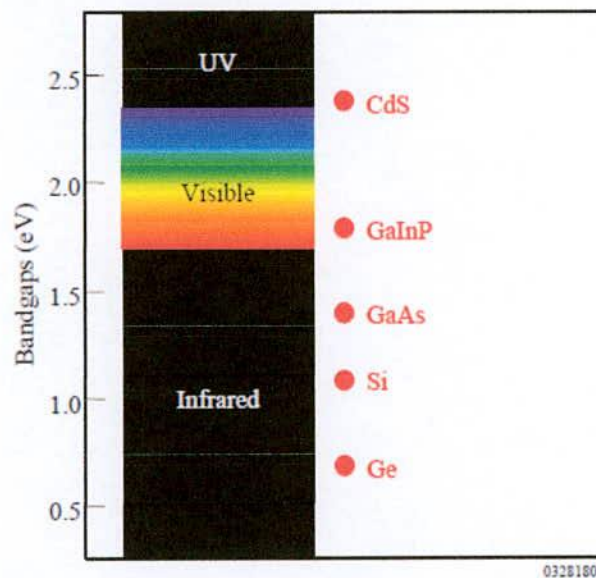


Figure 2.2: Comparison of band gap of common semiconductors and the electromagnetic spectrum [31].

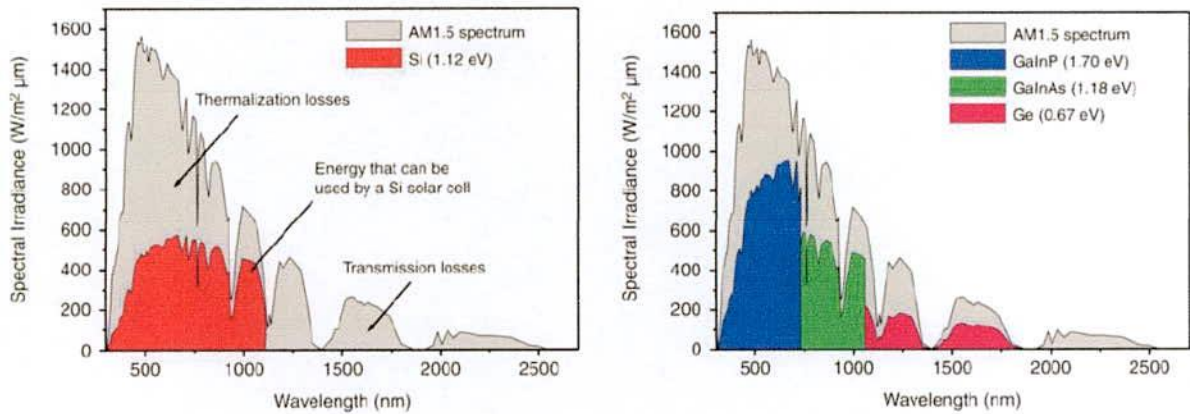


Figure 2.3: Solar irradiance absorption comparison of single junction-Si solar cell to common triple junction solar cell [32].

Solar cells are devices composed of semiconductors and are used to generate electric power when exposed to electromagnetic radiation. Based on the band gap of the materials used in creating the cells, not all the electromagnetic radiation may be used. That is, only certain parts of the electromagnetic spectrum may be used for solar cell technology due to the physical limitations of the semiconductor materials used. Figure 2.3 shows the solar radiation that is seen on earth and how different types of semiconductors absorb light. It can also be seen from the following figures that the peak irradiance occurs in the range of visible light (i.e. 380 - 750 nm). For this reason, solar cells are designed using the material or combination of materials so that the whole spectral irradiance can be absorbed [32].

2.3 Physical Representation of a Solar Cell

A simple solar cell uses a metallic grid to form one of the electrical contacts. The light enters into the semiconductor between the grid lines and be absorbed and converted into electrical energy. An antireflective layer is fabricated between the grid lines to limit reflection and increase the amount of light absorbed by the cell [33]. The metal grid and the antireflective

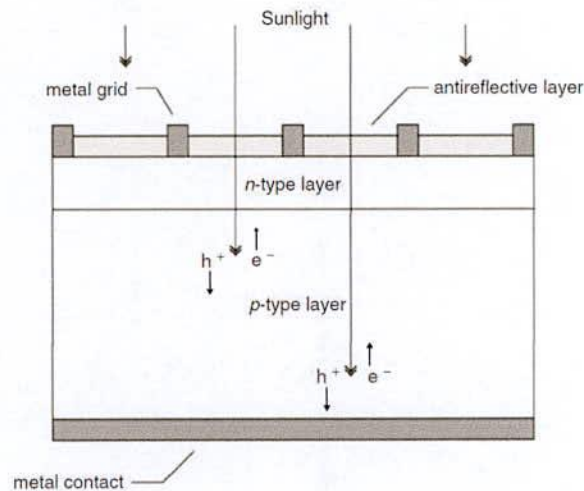


Figure 2.4: Schematic of a typical solar cell [33]

coating is fabricated over the p-n junction. A p-n junction is the most fundamental part of solar cell. The cell is fabricated through diffusion, ion implantation, or epitaxial methods. Figure 2.4 shows the physical structure of a basic solar cell.

Solar cells can be fabricated with a number of semiconductor materials. The most commonly used are the forms of silicon: monocrystalline, polycrystalline, and amorphous.

- ❖ **Monocrystalline-** The crystal lattice of the solid is continuous and unbroken to its edges. The monocrystalline solar cell can have up to 24% efficiency although they are more expensive than polycrystalline and amorphous solar cells [34].
- ❖ **Polycrystalline-** Composed of many small regions of single crystal materials. Polycrystalline solar cells have lower efficiency and low cost than monocrystalline solar cells. Their efficiency is up to 20%. Commercially available solar panels are made from polycrystalline solar cells [35].
- ❖ **Amorphous-** Contains no periodic structure unlike the other types of solids. It is commonly used to build thin film solar cells (a solar cell that is made by depositing

one or more thin layers of PV materials on a substrate). Amorphous is the cheapest of these three silicon based options with least efficient.

Silicon is used because its absorption characteristics are a good match to the solar spectrum. It is extensively used in the semiconductor industry and its fabrication technology. Solar cells can also be constructed using compound semiconductors InGaN, InGaAs, GaAs, GaInP, Cu(InGa)Se₂, and CdTe.

2.4 Working Principle of Solar Cell

Semiconductor solar cell is fundamentally simple device and delicately designed for efficiently absorb sun light and then convert it into electrical energy. A solar cell is simply a semiconductor p-n junction diode that can separate and collect electrons and holes and conducts the generated current in a specific direction [36].

A simplified schematic diagram of a typical solar cell is shown in figure 2.5. Consider a p-n junction with a very narrow and more heavily doped n-region. The light is illuminated through the thin n-side. The depletion region extends primarily into the p-side. There is a built-in field E_0 in this depletion layer. The electrodes attached to the n-side must allow illumination to enter into the device. As the n-side is very narrow, most of the photons are absorbed within the depletion region, W and within the neutral p-side (L_p), and generate electron-hole pairs (EHP) in these regions. Thus the photo-generated EHPs in the depletion region are immediately separated by the built-in field E_0 which drifts them apart. The electron reaches at the neutral n-side whereupon it makes this region negative by an amount of negative charge ($-e$). Similarly, the hole reaches at the neutral p-side and thereby makes this

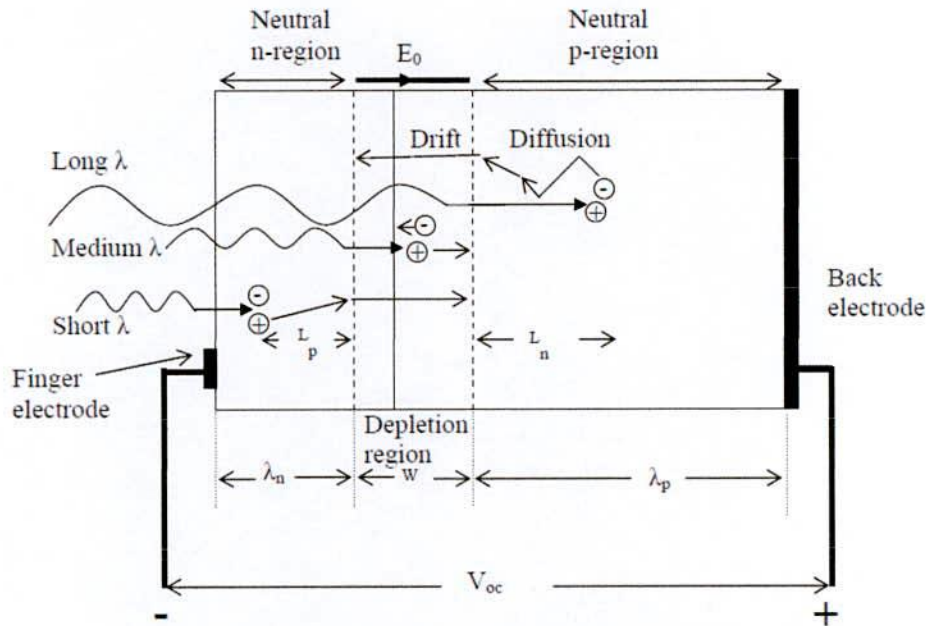


Figure 2.5: The working principle of solar cell.

side positive. Consequently, an open circuit voltage develops between the terminals of the device with the p-side positive with respect to the n-side. If an external load is connected, then the excess electron in the n -side can travel around the external circuit and reach the p-side to recombine with the excess hole there. It is important to realize that without the internal field E_0 it is not possible to drift apart the photo generated EHPs and accumulate excess electrons in the n-side and excess holes in the p-side.

The EHPs generated by long-wavelength photons in the neutral p-side diffuse around in this region as there is no electric field in this region. If the recombination lifetime of the electron is τ_n it diffuses a mean distance $L_n = \sqrt{2D_n\tau_n}$ where D_n is its diffusion coefficient in the p-side. The electrons within a distance L_n to the depletion region can readily diffuse and reach this region whereupon they become drifted by E_0 to the n-side as shown in figure 2.5. Consequently, only those photogenerated EHPs within the minority carrier diffusion length L_n to the depletion layer can contribute to the photovoltaic effect. Again the importance of the built-in field E_0 is apparent. Once an electron diffuses to the depletion region, it is swept over

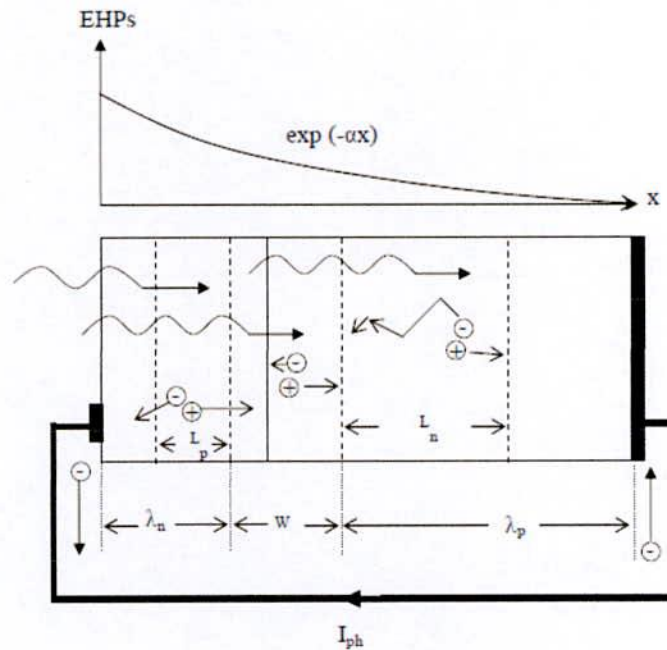


Figure 2.6: Solar cell operation.

to the n side by E_0 to give an additional negative charge there. Holes left behind in the *p-side* contribute a net positive charge to this region. Those photogenerated EHPs further away from the depletion region than L_n are lost by recombination. It is therefore important to have the minority carrier diffusion length L_n be as long as possible. The same ideas also apply to EHPs photogenerated by short wavelength photons absorbed in the n-side. Those holes photogenerated within a diffusion length L_p can reach the depletion layer and become swept across to the *p-side*. The photogeneration of EHPs that contributes to the photovoltaic effect therefore occurs in a region covering $L_p + W + L_n$. If the terminals of the device are shorted as in figure 2.6 then the excess electron in the n-side can flow through the external circuit to neutralize the excess hole in the p-side. This current due to the flow of the photogenerated carriers is called the photocurrent.

2.5 Efficiency Loss Factors in Solar Cell

The conversion efficiency of commercially available silicon solar cell is very poor. Extensive researches are being carried out for improving the efficiency up to its theoretical limit. Solar

cells manufactured through industrial process have efficiencies in the order 12 -15%. This means that about 88 - 85% losses occur in Si-based solar cells. It is therefore very much important to study different losses that occur in the solar cells and then find out the techniques that can be implemented for reducing different loss components in photovoltaics system.

2.5.1 Reflection Loss

The reflection loss occurs from the top surface through which light enter into the solar cell. Reflection mechanism reduces the absorbed carriers and hence the short circuit current I_{sc} . The losses due to reflection in a bare Si are about 30%. To reduce the reflectivity antireflective coating ARC (60nm) is deposited using CVD (chemical vapour deposition) and extruding (which is in the form of pyramids usually formed by etching the surface with the acid (H_2SO_4 or HNO_3 in H_2O_2) on top surface of the solar cells. Proper thickness and refractive index are important physical parameters for good ARC. Total internal reflection is desired when the photon strikes on the surface of the cell (interface between the Si and the ARC). The refractive index and thickness of the ARC material has to be adjusted to achieve internal reflection. The thickness of ARC layer is adjusted so that the reflected light from the ARC, interface of ARC, and Si will be out of phase resulting in destructive interference and leads to absorb maximum possible light in the cell.

2.5.2 Recombination Loss

Photon incident on the solar cell generates EHPs. Generated carriers need to be separated before recombination. Recombination causes loss of carrier and affects the performance of the cell. Open circuit voltage V_{oc} of the cell is reduced due to recombination of carriers. Different recombination losses that occur at different regions of the solar cells are: surface

recombination, bulk recombination, depletion region recombination, and recombination at metal Semiconductor interface. The recombination losses can be minimized using semiconductors having long life time for the photogenerated carrier. The elimination of all unnecessary defects could also be another solution.

2.5.3 Series and Shunt Resistance Losses

The series resistance gives rise to a voltage drop and therefore causes the deviation from ideal photovoltaic voltage-current characteristics. A fraction of the photogenerated carriers can also flow through the crystal surfaces (edge of the device) instead of flowing through the external load. It causes the effective internal shunt or parallel resistance that diverts the photocurrent away from the load. The series resistance can significantly deteriorate the solar cell performance by limiting the short circuit current. Similarly shunt resistance caused by extensive defects in the material also reduce the efficiency. Loss due to series (0.3%) and shunt (0.1%) resistances is negligible compared to other losses.

2.5.4 Inadequate Absorption of photons

Photons with energies larger than the band gap E_g of the semiconductor excite electrons from the valence band to the conduction band, resulting in free charge carriers; electrons and holes. If photons have energy exceeding semiconductor's band gap energy, the excess energy is usually dissipated as heat and thus wasted. In contrast, the photons whose energies are less than the band gap energy of the semiconductor are transmitted through the materials and are not used.

2.5.4 Thermal Losses

A significant portion of loss in solar cell is due to heat which is generated by the absorption energetic photons. The excess energy is released in the form of heat instead of EHPs

generation leads to rise of temperature in the cell. The parameters that are affected by the temperature of the cell are band gap energy, diffusion length, minority carrier lifetime, intrinsic carrier density, etc. resulting in increasing of reverse saturation current density. This leads to reduce open circuit voltage and degrades the efficiency of the cell.

Temperature effect is more pronounced in concentrator cells. Depending on the concentration ratio, temperature of the solar cell can rise above 1000°C and reduces the open circuit voltage. If temperature rise is kept within limits with the help of proper cooling arrangements (use of heat sinks or heat pipes) thermal losses could be maintained within limits.

2.5.6 Inadequate Assortment of EHPs

Any energy that an impinging photon has in excess of the energy gap of the material will contribute to the lattice vibration of the material and will eventually be dissipated as heat. On the other hand, a significant number of EHPs generated outside the space charge region can be separated by the built in field if they are generated within a diffusion length of the carrier. The majority of the EHPs generated far from the junction will recombine, causing the efficiency to fall below 100%.

2.5.7 Fill Factor (FF) Loss

It is extremely important to achieve high fill factors to maximize the power generation capabilities of the cell. The fill factor of silicon wafer solar cells is strongly influenced by recombination currents and ohmic resistances. It is defined as a measure of junction quality and series resistance of the cell. The function of the FF can be understood by realizing the I-V characteristics of solar cell as shown in figure 2.7 and is given by equation (1)

$$\text{Fill factor, } FF = (I_{mp} \times V_{mp}) / (V_{OC} \times I_{OC}) \quad (1)$$

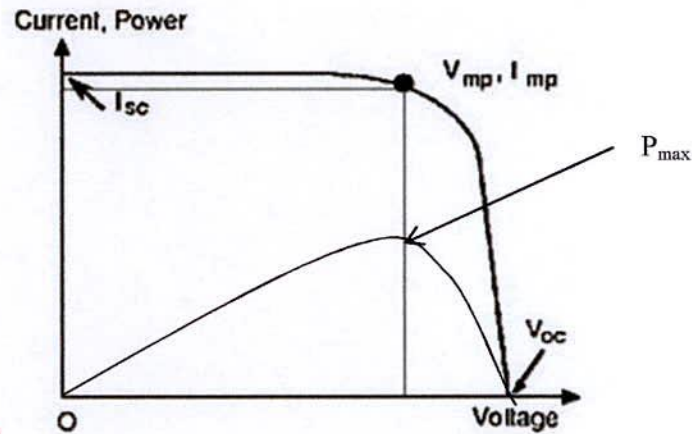


Figure 2.7: Current- voltage characteristics of a solar cell.

Fill factor loss is determined by the curvature of the current-voltage characteristic of the device. A device operating at V_{oc} results in all absorbed photons recombining radiatively and no current being extracted. All absorbed photons will be extracted at short circuit current (I_{sc}) however, this will only occur in the absence of luminescent radiation when the device is operated at zero volts. Fill factor loss is a result of operating at the maximum power point and has been calculated as shown in equation (2).

$$\text{Fill factor loss} = V_{OC} \times I_{SC} - I_{mp} \times V_{mp} \quad (2)$$

In a real solar cell this is affected by cell resistances however, in the ideal model used here the fill factor loss tends to zero for a cell at 0°K .

2.6 Efficiency Enhancement Techniques

Various losses occur in the Si solar cells are briefly discussed. Among them recombination, reflection, resistive, and thermal are the major loss components at 1 sun solar concentration. At higher concentration levels the resistive losses become dominant. Various schemes for reduction of losses have been suggested for the enhancement of efficiency limit. In this study we will discuss MJ technique. Other techniques are also briefly explained here.

2.6.1 MJ Solar Cell

MJSC consists of a multiple, single junction solar cells stacked on one another in which the bandgaps of the subcells are divided by tuning the composition. For efficient absorption of whole solar energies, the higher bandgap subcell is fabricated at the top and others are below the top subcell. Existing MJ devices have achieved efficiencies over 37% [20] and further improvement may be achieved by increasing the number of layers. Although MJSC provides us higher efficiency, it has an inherent drawback, that is, its efficiency is tied to the material quality and availability of suitable materials having band gap matched to the solar spectrum. Nowadays $\text{In}_x\text{Ga}_{1-x}\text{N}$ is a promising material and its bandgap energy can be tuned from 0.64 to 3.4eV [37] and suitably matched with the solar spectrum.

2.6.2 Multiple Spectrum Solar Cell

Multiple spectrum solar cells take the input solar spectrum, and change it to a new spectrum with the same power density. The main feature of these approaches, which include up and down-conversion [11] and thermo-photonics, is that the transformation of the solar spectrum is done separately from the solar cell itself, thus increasing the efficiency of an existing solar cell structure via additional coatings. This technology could be applied to any solar cell provided that power gained through spectral alternation offsets the cost of the additional optical coating. As many of the suggested approaches can potentially be implemented in a low cost fashion, multiple spectrum photovoltaic system primarily offer a mechanism for relatively moderate efficiency increases using existing solar cell technology as shown in figure 2.8. Here the up/down conversion can be implemented by either material systems or by using quantum wells/ quantum dots approaches.

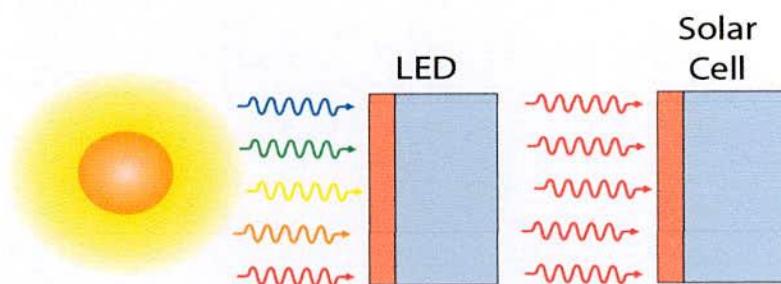


Figure 2.8: Multiple spectrum photovoltaic system

2.6.3 Compound Absorption Path Solar Cell

Existing solar cell approaches is the one-to-one relationship between an absorbed photon and a generated electron-hole pair. This relation can be circumvented via two mechanisms (i) two-photon absorption and (ii) impact ionization/auger generation as shown in figure 2.9. Although such absorption processes have been measured in bulk materials [38], nano-structured materials are required in order to measure a large effect. For example, nano-structured materials have high two-photon absorption and impact ionization processes, with close to 100% impact ionization reported [39]. While high impact ionization rates are an important first step, such high rates alone do not insure high solar cell efficiency, and the critical measurement for such devices is to demonstrate quantum efficiencies substantially exceeding unity.

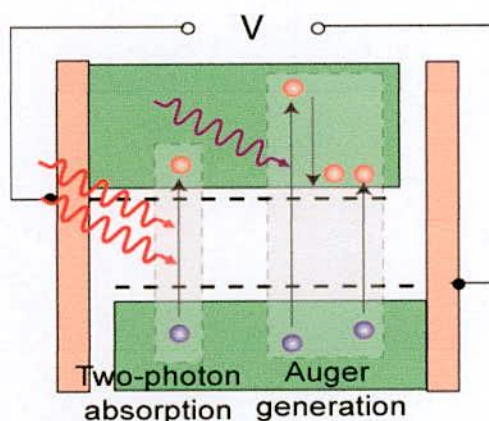


Figure 2.9: Absorption in compound absorption path solar cell

2.6.4 Multiple Energy Level Solar Cells

In multiple energy levels solar cell, the mismatch between the incident energy of the solar spectrum and a single band gap is accommodated by introducing additional energy levels such that photons of different energies can be efficiently absorbed. Multiple energy levels solar cell can be implemented either as localized energy levels (first suggested as a quantum well solar cell) or as continuous mini-bands (also called intermediate band for the first solar cell to suggest this approach) as shown in figures 2.10 (a) & 2.10 (b). Both cases, which are shown in figure 2.10, have a fundamental similarity in that the key issue is the generation of multiple light-generated quasi-Fermi levels. The transport of the carriers between the two approaches, however, is substantially different. In the mini-band case, the transport must occur along the mini-bands and hence the carriers must not be able to thermalize from one band to another. This means that the density of states must be zero between the bands, and such approaches must use either quantum dots or a material which inherently has multiple bands. In localized energy level approaches, transport is accomplished by having the carriers at each localized energy level escape by light absorption. To maintain high collection efficiency, the escape time should be faster than the recombination time. The feasibility of the

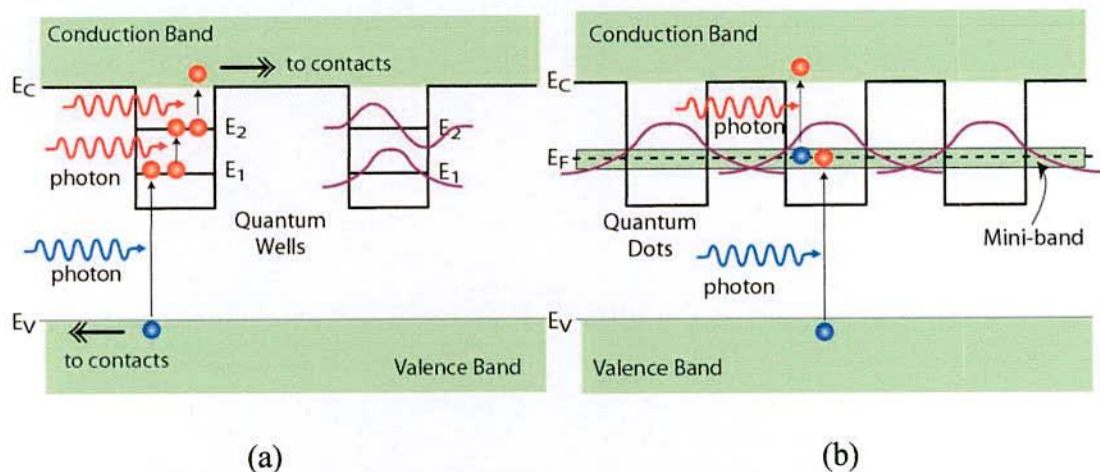


Figure 2.10: Operation of multiple energy level solar cells as (a) quantum well solar cell & (b) intermediate band solar cell.

escape process is well demonstrated by quantum-well infrared photodetectors, which have high collection from intra-sub band processes. Localized band approaches have a further advantage in that successive localized energy levels can have different energies, thus allowing the a large number of effective band gaps and high efficiencies.

2.6.5 Multiple Temperature Solar Cells

Figure 2.11 shows that a solar cell which contains multiple temperatures in a single device can use these temperature differentials to generate power. The multiple temperatures may be due to variations in the physical temperature of the lattice, but it is easier to maintain a temperature differential between hot carriers and thermalized carriers. The multiple temperature approach has the advantage that a thermal converter allows higher efficiencies given identical high concentration structures. A thermal converter can be implemented by a structure in which the band edges in the converter vary, allowing interactions between hot carriers and carriers at the band edge. While this approach allows efficiencies 66% with three energy levels, the physical effect of thermal interactions have not been demonstrated.

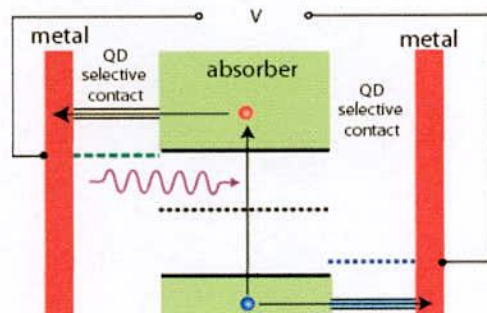


Figure 2.11: Concept of multiple temperatures solar cells

2.7 Important Fabrication Issues in MJSC

A MJSC solar cell experiences four major fabrication challenges. These are band gap, lattice matching, current matching and tunnel junctions, which are discussed in the following

section. Appropriate band gap selection and lattice matching are the key points for designing efficient MJSC.

2.7.1 Bandgap Issue

In order to improve conversion efficiency of a photovoltaic cell, the solar cell should absorb as much of solar energy as possible. The bandgap separation of adjacent layers should be as small as possible, because instead of generating EHPs the absorption of high energy photons generates heat energy in the lattice structure of absorbing material [40]. For efficient utilization of solar energy in different subcells of MJSC, the top layer should be higher bandgap material and the bottom layer should be smaller bandgap. The availability of suitable materials that nicely matched to solar spectrum and bandgap stepping in different subcells are main design hinders in MJSC approach.

2.7.2 Lattice Mismatch Issue

The lattice constant is the distance between two atoms in a crystal structure. It is desirable to have epitaxial layers under lattice matching condition. Because, quality of epitaxial layer/ junction/ interface is highly dependent on the matching of lattice constant between two layers. In case of MJSC different subcells are grown epitaxially with different bandgap materials in order to complete absorption of solar energy. This implies that the material used in different subcells must have different lattice constants.

Researchers at the national renewable energy laboratory (NREL) showed that a lattice mismatch as small as 0.01% significantly decreases the current produced by the solar cell. The relationship of bandgap energy with lattice constant of different semiconductors is shown in figure 2.12. In case of the proposed InGaN-based MJSC structure, the lattice constant

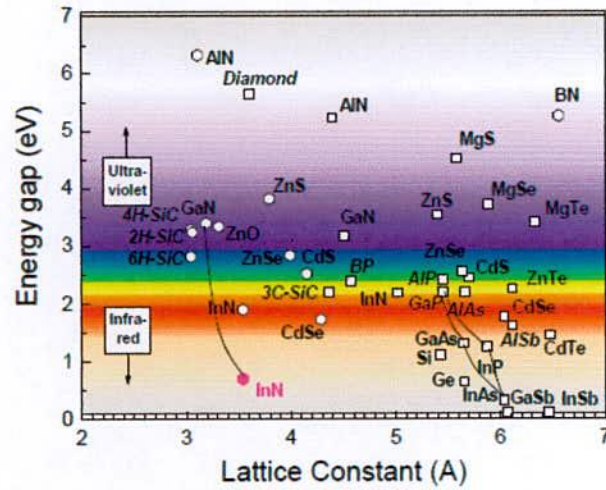


Figure 2.12: Relationship between bandgap energies and lattice constants of different semiconductors.

decreases in different layers from bottom to top that leads to induce tensile strain due to layered change in lattice constants from bottom to top subcells. It is well known that the strain induced due to the change in lattice constant between two layers can easily be determined using in epitaxial strain model [41]. However, residual strain induced due to the change in lattice constants in multiple layers can not be determined using simple epilayer strain model. Further, the bandgap in semiconductor material is modified under the influence of strain [41]. Therefore, to understand the actual efficiency in MJSC, it is very much important to determine MJSC structure dependent state of strain and hence to investigate the efficiency of MJSC including the strain effect.

2.7.2.1 Energy Bandgap under the Influence of Strain

It is well established that the bandgap energy is modified under the influence of strain in semiconductor materials depending on the state of strain [27], [41]. The energy band gap of InGaN decreases under the application of tensile strain, whilst a compressive strain causes an increase of the band gap energy of the same material [25].

2.7.3 Current Matching Issue

The serial architecture of monolithically grown multijunction solar cells makes matching of currents into a desirable characteristic. The output current of the multijunction solar cell is limited to the smallest current produced by any of the individual junctions. If this is the case, the currents through each of the subcells are constrained to have the same value. The current is proportional to the number of incident photons exceeding the semiconductor's bandgap, and the absorption constant of the material. A layer must be made thinner if the photons that exceed the bandgap are in abundance. At the same time, a layer with a low absorption constant must be made thicker, since on average a photon must pass through more of the material before being absorbed. After materials are selected with desired bandgaps and lattice constants, the thickness of each layer must be determined based on the material's absorption constant and the number of incident photons with a given energy, so that each layer will generate the same photocurrent. The absorption constant for various semiconductors as a function of photon wavelength is shown in figure 2.13.

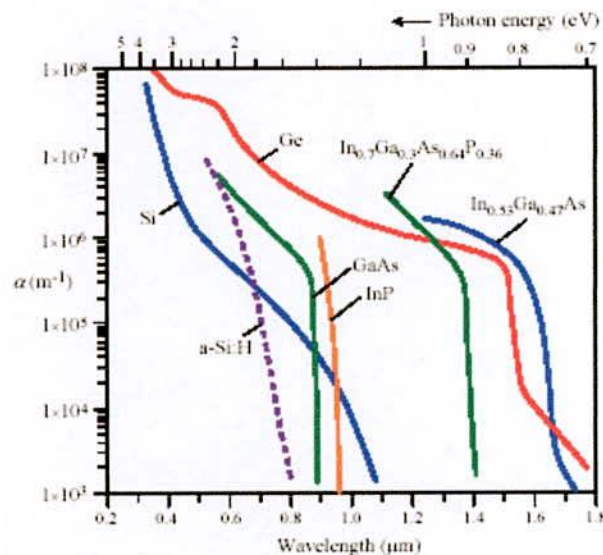


Figure 2.13: Absorption coefficient versus wavelength for various semiconductor materials [43].

2.7.4 Use of Tunnel Junction

Tunnel junctions (TJs) are key components to the successful operation of multijunction solar cells (MJSCs) under high concentration. Ideally, they serve as perfectly transparent, highly conductive interconnections between adjacent subcells [40]. For optimal performance, the peak tunneling current density J_{peak} must be significantly higher than the short-circuit current density J_{sc} of the solar cell to minimize series resistance contributions and avoid a degradation of the maximum power point. Since the J_{sc} of an MJSC scales linearly with concentration as shown in figure 2.14, conditions resulting in a value of J_{sc} greater than the TJ J_{peak} can be occurred if the TJ is performing poorly or if a cell is operated well beyond the level of concentration [44].

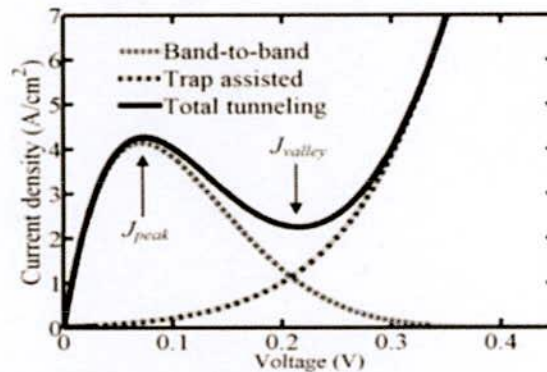


Figure 2.14: Current density–Voltage (J – V) characteristic of a tunnel junction

One problem encountered when creating a tunnel junction is that when the cell is annealed at high temperature, the tunnel junction may diffuse out of the junction, widening the depletion region. The wide depletion region reduces tunnelling and limits the current that can be carried in the cell.

2.8 Typical MJSC Structure

The energy from incoming photons must have enough energy to excite electrons from the valence band sufficient energy to move to the conduction band. But the solar spectrum contains photons of different energies; as a result, a single p-n junction solar cell will give

limited range of conversion efficiency due to inefficient utilization of solar energy. The solution of poor conversion efficiency is to absorb a wider range of the solar spectrum using multiple p-n junctions stacked with different bandgaps. This idea is referred to as MJSC [42]. Each layer is made of a different material, which is usually III-V semiconductor, and absorbs a different portion of the spectrum. The top layer has the largest band gap so that only the most energetic photons are absorbed in this layer. Less energetic photons must pass through the top layer since they are not energetic enough to generate EHPs in the material. Each layer going from the top to the bottom has a smaller band gap than the previous. Therefore, each layer absorbs the photons that have energies greater than or equal to the band gap of that layer and less than the band gap of the higher layer as shown in figure 2.15 (a). In this way there arises a perfect utilization of the full solar spectrum and increased efficiency. For an instance, a typical InGaP-based MJSC model in according to the multijunction principle is presented in figure 2.15 (b). The subcells are placed from bottom to top with lower to higher bandgap by adjusting the composition. The window layer is used at the top to reduce surface recombination, on the other hand, back surface field (BSF) at the bottom to reduce carrier scattering. The function of high bandgap window is also to reduce the cell's series resistance. In addition to window and BSF layers tunnel junctions are used in this model to provide low electrical resistance and to create optically low loss path between two subcells.

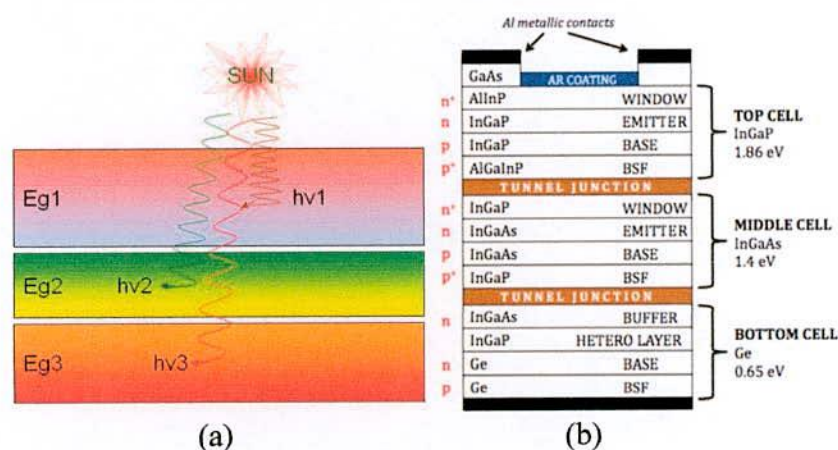


Figure 2.15: (a) Multijunction principle representation. (b): InGaP-based Multijunction Solar Cell.

2.9 Strain in Multi-layered Structure

In case of a multilayer structure, the lattice constant in different subcells are different in magnitudes due to the variation of their band energies and compositions as shown in figure 2.16 (a). For this reason, lattice mismatch arises between the adjacent layers. In order to make a MJSC structure the higher bandgap subcells are placed at the top and lower at the bottom. As a result high energetic photons will be absorbed in the top cell and remaining photons will be absorbed in the subsequent adjacent subcells depending on the band gap energy of the subcells.

In order to absorb the whole solar energy using $\text{In}_x\text{Ga}_{1-x}\text{N}$ -based MJ solar cell structure, GaN subcells having higher band gap energy must be placed at the top InN subcell at the bottom and other $\text{In}_x\text{Ga}_{1-x}\text{N}$ subcells with different compositions will be placed in between top and bottom cells depending on the subcells energies. It is well known that the InN and GaN material provide lattice constant 3.548\AA and 3.189\AA respectively.

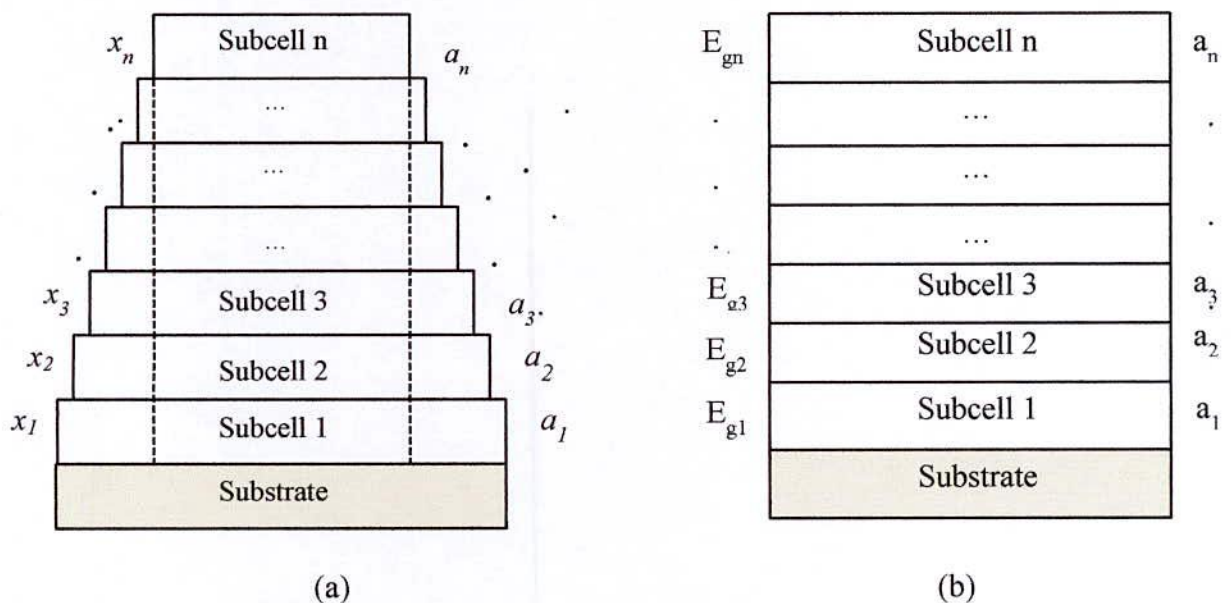


Figure 2.16: (a) Individual subcell with different composition, corresponding lattice constant.

(b) Multilayer Structure having different subcell bandgap energies.

If an epitaxial layer of $\text{In}_x\text{Ga}_{1-x}\text{N}$ is grown on the InN layer, tensile strain is induced. Therefore, decreasing of lattice constant from bottom to top layer in case of $\text{In}_x\text{Ga}_{1-x}\text{N}$ -based MJSC structure leads to tensile strain in each layer. Figures 2.16(a) and 2.16(b) show an overview how strain is induced due to layered change in lattice constant in $\text{In}_x\text{Ga}_{1-x}\text{N}$ -based MJSC structures.

CHAPTER III

Multijunction Solar Cell Structure and Strain Model

3.1 Introduction

To be competitive with the conventional energy resources, the conversion efficiency of the solar cells must be improved. Multijunction solar cell (MJSC) technology offers high efficiency compared to traditional single junction solar cells [9]. The group-III nitride compounds and their alloys have recently been received considerable attention for solar cell applications. Specially, $\text{In}_x\text{Ga}_{1-x}\text{N}$ (0.64 to 3.4 eV) is a promising material for MJSC, because its bandgap energy is nicely matched to solar spectrum [37]. This creates an opportunity to design and fabricate $\text{In}_x\text{Ga}_{1-x}\text{N}$ -based MJSCs with improved performance. In MJSC technology, the subcells are grown epitaxially with different energy bandgaps, which lead to change lattice parameters in different layers. As a result residual strain is induced in different layers of MJSC. Three different MJSC structures named MJSC-1, MJSC-2 and MJSC-3 are investigated. For better coupling of light, current matching, reduction of carrier scattering and providing low loss optical path, window layer, tunnel junction and BSF layer are placed in different positions of different MJSC structures.

It is well known that change in lattice constant between two layers induces strain in semiconductor junctions and can be easily determined using epilayer strain model [41]. On the other hand, if strain is induced in bulk crystal due to continuous variation of composition

along the growth direction or radial direction, well established strain model for bulk-crystal can be used [27]. In our case, strain is induced due to the change in lattice constants in different layers of MJSC structure. To determine the strain in our case, multi-layered strain model can be used [28].

3.2 Properties of $\text{In}_x\text{Ga}_{1-x}\text{N}$

The theoretical efficiency limits of solar energy conversion are strongly dependant on the range and number of different band gaps or effective band gaps that can be incorporated into a solar cell. For tandem devices, the range of band gaps available as well as the ability to achieve junctions with specific band gaps and device structures is critical in achieving high efficiency. A fundamental limitation in achieving ultra-high efficiency solar cells (> 50%) is the availability of materials and corresponding device structures. The $\text{In}_x\text{Ga}_{1-x}\text{N}$ material system offer substantial potential in developing ultra-high efficiency devices. The recent measurements indicate that the band gap of InN is lower than that of reported previously. Due to other unique material properties, such as absorption coefficient, defect density, doping etc. make it promising for advanced solar cell.

A short description of bandgap energy, absorption coefficient and some other parameters of $\text{In}_x\text{Ga}_{1-x}\text{N}$ material discussed in the next section.

3.2.1 Band Gap Energy

The composition-dependent bandgap energy of ternary compound $\text{In}_x\text{Ga}_{1-x}\text{N}$ is essential for designing of multi-layered structures. The band gap energy of unstrained InGaN as a function of alloy composition can be expressed [38] by equation (3)

$$E_{g\text{InGaN}} = (1 - x)E_{g\text{GaN}} + xE_{g\text{InN}} - bx(1 - x) \quad (3)$$

where, the energy gaps of binaries $E_{g_{GaN}}$ and $E_{g_{InN}}$ are equal to 3.4 and 0.64 eV [30], respectively and bowing parameter $b = 3.5\text{eV}$ [26]. The variation of band gap energy of $\text{In}_x\text{Ga}_{1-x}\text{N}$ material as a function of composition is shown figure 3.1.

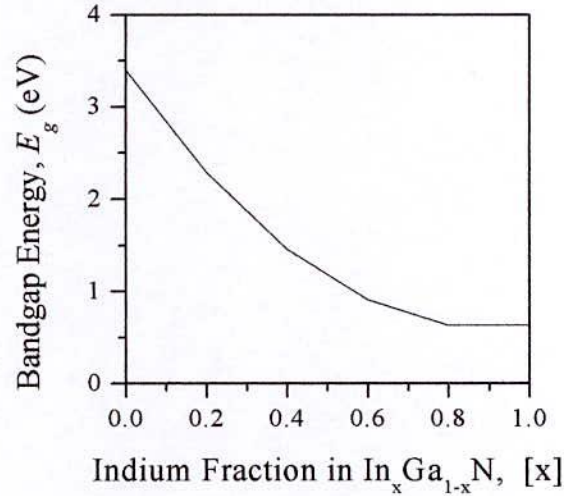


Figure 3.1: Compositional dependence of bandgap energy of InGaN material.

In this study, the subcells are placed from bottom to top with lower to higher bandgaps by adjusting the composition. The splitting of bandgaps for 3, 5, and 7 subcells are shown in Table 3.1 [40].

Table 3.1: Bandgap energy distribution of different subcells of MJSC

No. of Stack	Values of Bandgap (eV)
3	0.952 1.372 1.899
5	0.92 1.166 1.44 1.757 2.21
7	0.706 0.932 1.135 1.355 1.588 1.888 2.32

3.2.2 Absorption Coefficient α

When light impinges on a semiconductor with photon energy, $h\nu$, greater than or equal to the band gap energy, E_g , the light is absorbed resulting in excitation of an electron from the valence band to the conduction band. The absorption coefficient, α , is a material parameter

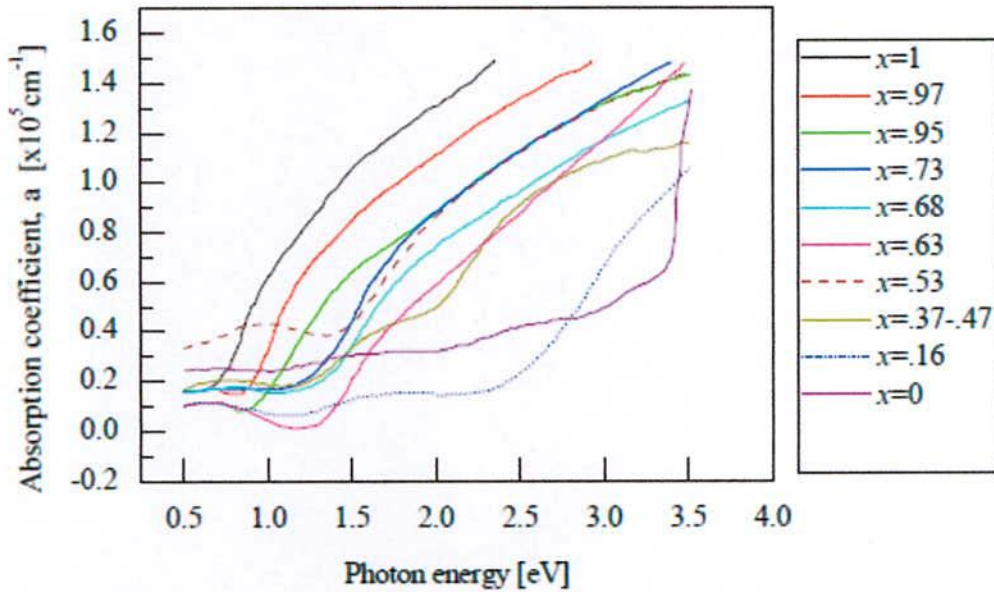


Figure. 3.2: Room temperature absorption coefficient of $\text{In}_x\text{Ga}_{1-x}\text{N}$ alloys as a function of photon energy with different indium composition, x [45].

which depends on the photon energy. It is a measure of how good the material is for absorbing light of certain wavelength. Absorption coefficient in $\text{In}_x\text{Ga}_{1-x}\text{N}$ is related to its composition i.e. In fraction, x , as well as wave length of the light. It also depends on the operating temperature. Room temperature (300°K) [45] absorption coefficient of $\text{In}_x\text{Ga}_{1-x}\text{N}$ as a function of photon energy with different indium composition is shown in figure. 3.2.

3.2.3 List of Important Parameters

InN possesses a strong propensity for n-type conductivity which can be explained by an exceptionally high Fermi stabilization energy well above the conduction band minimum. On the other hand GaN possesses higher carrier mobilities, high current density and also provide lighter devices. Their combination makes a composition dependent compound $\text{In}_x\text{Ga}_{1-x}\text{N}$ which has significant use in the tandem solar cell.

In this study, the experimental measurements of all parameters are not available for the ternary compound $\text{In}_x\text{Ga}_{1-x}\text{N}$. In our study, the parameters which are not available for InGaN

Table 3.2: Properties of GaN and InN materials [46-49]

Parameters	Notation	InN	GaN
Bandgap (eV)	E_g	0.64	3.4
Lattice constant (a_0)	a	3.548	3.189
Young's modulus	E	141	270
Poission's ratio	ρ	0.21	0.18
Dielectric constant	ϵ	14.6	10.4
Elastic constants (GPa)	C_{11}	223	367
	C_{12}	114	135
	C_{13}	92	103
	C_{33}	224	405
Deformation potentials (eV)	D'_1	5.81	3.62
	D'_2	8.92	4.60
	D_3	5.47	2.68
	D_4	-2.98	-1.74
Density of state (cm^{-3})	N_C	$1.76 \times 10^{14} \times T^{3/2}$	$4.3 \times 10^{14} \times T^{3/2}$
	N_V	$10^{16} \times T^{3/2}$	$8.9 \times 10^{15} \times T^{3/2}$
Diffusion Length (cm)	L_n	2.8×10^{-6}	125×10^{-6}
	L_p	0.16×10^{-7}	79×10^{-6}
Diffusion Coefficient (cm^2/s)	D_n	8	25
	D_p	1.6	9
Absorption Coefficient(cm^{-1})	α	6×10^4	10^5

crystal are determined by linear interpolation between the values measured experimentally for the binaries GaN and InN. Table 3.2 shows some important parameters which are taken from the references [46-49].

3.3 InGaN-based MJSC Structures

The MJSC structures studied here are shown in figures 3.3(a-c) [22-24]. The subcells are placed from bottom to top with lower to higher bandgap by adjusting the composition. In MJSC-1, the window layer is used at the top to reduce surface recombination, on the other hand, back surface field (BSF) at the bottom to reduce carrier scattering [49]. The function of high bandgap window is also to reduce the cell's series resistance. In addition to window and BSF layers tunnel junctions are used in MJSC-2 to provide low electrical resistance and optically low loss path between two subcells [23]. Each unit cell is comprised of a window,

BSF and tunnel junction in MJSC-3 structure [22]. The bandgaps used in 3, 5, and 7 subcells of different MJSC structures are listed in table 3.1. The bandgap of the material used in the window, tunnel junction, and BSF layers must be higher than the bandgap of adjacent subcell.

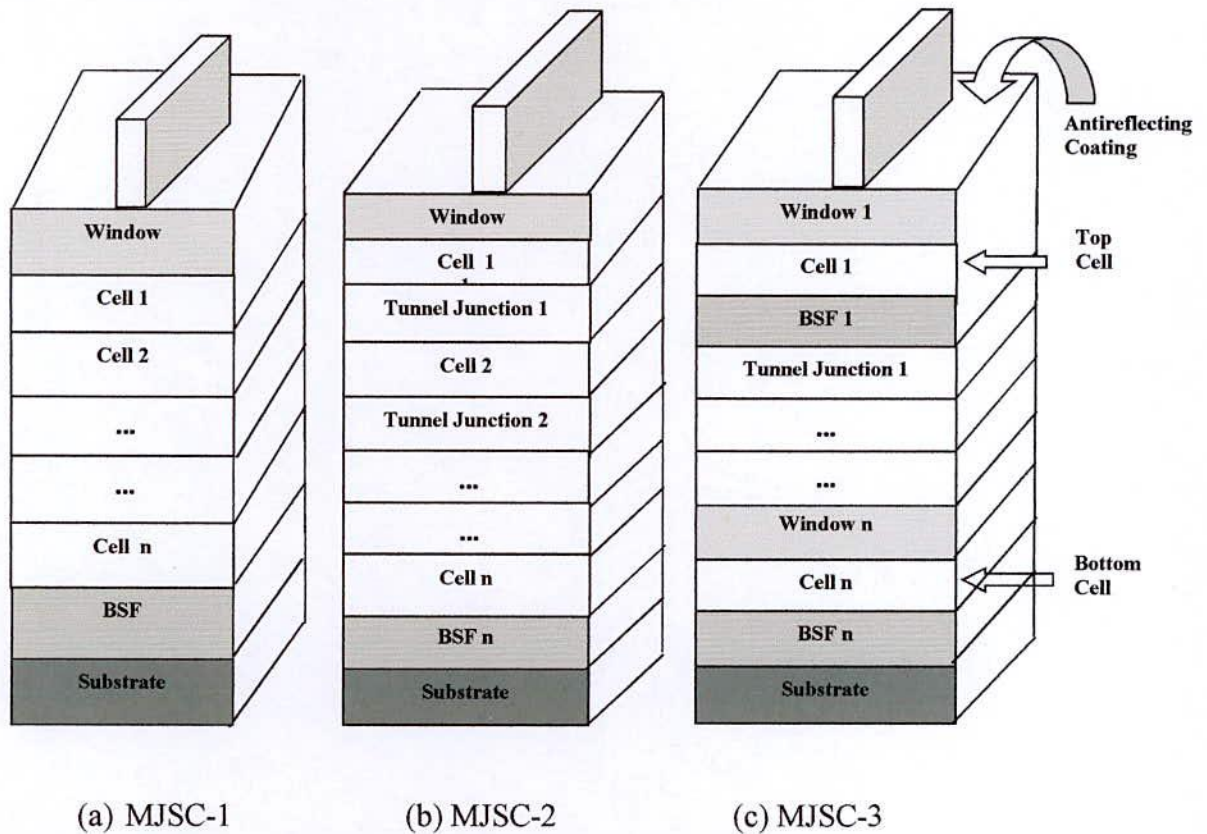


Figure 3.3: The schematic illustration of (a) MJSC-1, (b) MJSC-2 and (c) MJSC-3 [22-24].

3.4 Multi-layered Strain Model

The multilayered strain model is developed [28] based on the multilayer structure shown in figure 3.4. The position and thickness of the layers are indicated by y_n and t_n , respectively. A sacrificial layer is used to reduce lattice mismatch between the substrate and layer-1. Layer-1 to layer-n consists of multi-layers that lead to induce residual strain due to change in lattice constant in different layers. Since the MJSC structure have different layers with layered change in lattice constant multi-layer strain model can be used to determine strain in MJSC structure.

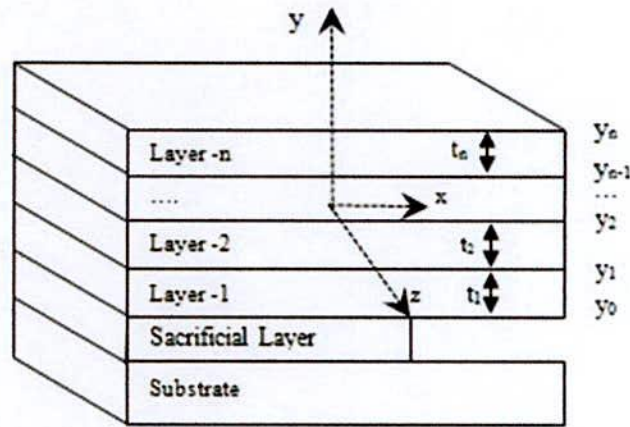


Figure 3.4: Multilayer structure with n-layer

The plane strain induced in multilayered system due to the change in lattice constant in different layers can be given [24].

$$\varepsilon = k + \frac{y-y_b}{G} \quad (4)$$

where k is the uniform strain component and G and y_b is the parameters that can be given [24] by

$$y_b = \frac{\sum_{i=1}^n E'_i t_i (y_i + y_{i-1})}{\sum_{i=1}^n E'_i t_i} \quad (5)$$

The other parameters are determined by the following equations,

$$G = \frac{-2 \sum_{i=1}^n E'_i t_i [y_i^2 + y_i y_{i-1} + y_{i-1}^2 - 3y_b (y_i + y_{i-1} - y_b)]}{3 \sum_{i=1}^n E'_i t_i (y_i + y_{i-1} - 2y_b (k - \eta_i \varepsilon_i^0 + \nu_i d))} \quad (6)$$

and

$$k = \frac{\sum_{i=1}^n E'_i t_i (\eta_i \varepsilon_i^0 - \nu_i d)}{\sum_{i=1}^n E'_i t_i} \quad (7)$$

where, thickness of each layer $t_i = y_i - y_{i-1}$. E_i and ν_i are Young's modulus and Poisson's

ratio. $E'_i = E_i/(1 - v_i^2)$. Here $\eta_i = 1 + v_i$ and ε_i^0 is the initial strain. The parameter d can be given by

$$d = \frac{(a_{12}-a_{11})a_{23}b_1 - (a_{21}b_1 - a_{11}b_2)}{(a_{11}a_{22} - a_{12}a_{21})a_{22} + (a_{12}^2 - a_{11}^2)a_{23}} \quad (8)$$

The parameters including the expression of d can be obtained by the following linear system of algebraic equations,

$$\begin{bmatrix} a_{11} & a_{12} & 0 \\ a_{21} & a_{22} & a_{23} \\ a_{31} & a_{32} & a_{33} \end{bmatrix} \begin{Bmatrix} k \\ d \\ R \end{Bmatrix} = \begin{Bmatrix} b_1 \\ b_2 \\ b_3 \end{Bmatrix} \quad (9)$$

where,

$$a_{11} = a_{32} = \sum E'_i t_i$$

$$a_{12} = a_{31} = \sum E'_i t_i v_i$$

$$a_{21} = \sum E'_i t_i (y_i^m - y_b)$$

$$a_{22} = a_{33} = \sum E'_i t_i v_i (y_i^m - y_b)$$

$$a_{23} = \frac{1}{3} \sum E'_i t_i [4(y_i^m)^2 - y_i y_{i-1} - 3y_b(2y_i^m - y_b)]$$

$$b_1 = b_3 = \sum E'_i t_i \eta_i \varepsilon_i^0$$

$$b_2 = \sum E'_i t_i \eta_i \varepsilon_i^0 (y_i^m - y_b)$$

R is curvature and $y_i^m = \frac{(y_i + y_{i-1})}{2}$. Curvature R is the reciprocal of curvature radius G :

$R=1/G$. Using equation (4) the strain can be calculated for different MJSC structures as a

function of number of layers. The composition-dependent Young's modulus and Poisson's ratio for InGaN can be determined by linear interpolation between the values listed in table 3.2 for binaries GaN and InN [26].

3.5 Strain-Induced Change in Energy Bandgap

It is well established that the bandgap energy is modified under the influence of strain in semiconductor materials depending on the state of strain [27, 41]. Under the influence of tensile strain the bandgap energy of InGaN is reduced [51]. The strain-induced change in bandgap energy, ΔE_{gs} can be given [26] by

$$\Delta E_{gs} = 2[-(D'_2 + D_4) + (D'_1 + D_3) \frac{C_{13}}{C_{33}}] \varepsilon \quad (10)$$

where ε is the subcell position-dependent in plane strain. D'_1 , D'_2 , D_3 , and D_4 are the deformation potentials, and C_{13} and C_{33} are the elastic constants. The experimental measurements of these parameters are not available for InGaN material. Therefore, the parameters used here are determined by linear interpolation between the values available for GaN and InN materials and are listed in table 3.2. Substituting the subcell position-dependent strain in equation (10) the strain-induced change in bandgap energy corresponding to each subcell can be determined. Since the relaxed bandgap energy, E_g is reduced under the influence of tensile strain, the bandgap energy under strained condition can be expressed by

$$E_{gs} = E_g - \Delta E_{gs} \quad (11)$$

3.6 Photo-current Density:

The photocurrent is induced in a subcell of the MJSC structure by the absorption of photons having energies greater than or equal to the bandgap energy of the subcell. The total photo

current density at a given wavelength is the sum of hole $J_{pi}(\lambda)$, electron $J_{ni}(\lambda)$ and depletion region $J_{dr}(\lambda)$ current densities and can be represented [22, 49] by

$$J_{phi} = \sum_{AM 1.5} J_{pi}(\lambda) + J_{ni}(\lambda) + J_{dr}(\lambda), E_g(i) \leq h\nu \quad (12)$$

where,

$$J_{pi}(\lambda) = \left\{ \frac{qF(1-R)\alpha L_p}{\alpha^2 L_p^2 - 1} \right\}$$

$$\times \left[\frac{\left(\frac{S_p L_p}{D_p} + \alpha L_p \right) - e^{-\alpha x_j} \left\{ \frac{S_p L_p}{D_p} \cosh\left(\frac{x_j}{L_p}\right) + \sinh\left(\frac{x_j}{L_p}\right) \right\}}{\frac{S_p L_p}{D_p} \sinh\left(\frac{x_j}{L_p}\right) + \cosh\left(\frac{x_j}{L_p}\right)} - \alpha L_p e^{-\alpha x_j} \right]$$

$$J_{ni}(\lambda) = \left\{ \frac{qF(1-R)\alpha L_n}{\alpha^2 L_n^2 - 1} \right\} e^{-\alpha(x_j+W)} \times \left[\alpha L_n - \frac{\left(\frac{S_n L_n}{D_n} \right) [\cosh(H'/L_n) - e^{-\alpha H'}] + \sinh(H'/L_n) + \alpha L_n e^{-\alpha H'}}{\frac{S_n L_n}{D_n} \sinh(H'/L_n) + \cosh(H'/L_n)} \right] \text{ and}$$

$$J_{dr}(\lambda) = qF(1-R)e^{-\alpha x_j} [1 - e^{-\alpha W}]$$

Here i is an integer and indicates the number of layer/junction of MJSC. α is the absorption coefficient, F is the number of incident photons/cm²/s per unit bandwidth and R is the fraction of these photons reflected from the surface. F is calculated from the solar energy spectrum (AM of 1.5) shown in figure 3.5.

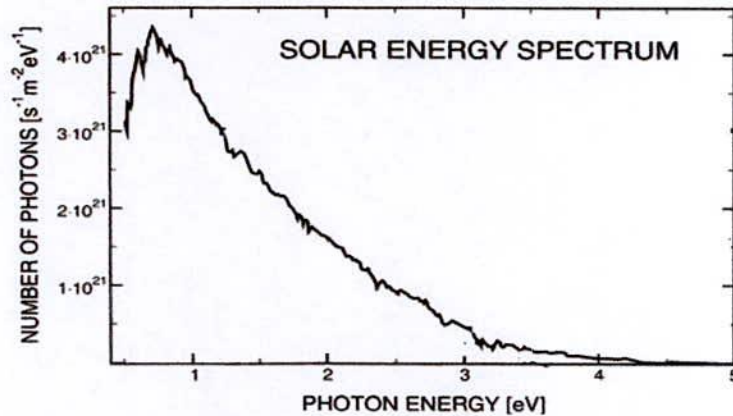


Figure 3.5: Solar energy spectrum (AM of 1.5) in terms of photon vs. photon energy [52].

The depletion width W can be represented by

$$W = \left\{ \frac{2\varepsilon V_0}{q} \left[\frac{1}{N_A} + \frac{1}{N_D} \right] \right\}^{1/2} \quad (13)$$

where, V_0 is the contact potential, ε is di-electric constant, q is the elementary electron charge. The concentration of acceptor and donor atoms per cm^3 on the p-side and n-side are denoted by N_A and N_D respectively.

For a typical p-n junction, contact potential V_0 can be given by

$$V_0 = \frac{KT}{q} \ln \frac{N_A N_D}{n_i^2} \quad (14)$$

where, K , T , and q are the Boltzmann constant, temperature, and elemental charge respectively.

3.7 Strain Effect on Open Circuit Voltage

Taking into account of strain effect, the open circuit voltage of a subcell can be obtained from

$$V_{OC} = \frac{KT}{q} \ln \left(\frac{J_{phi}}{J_0} + 1 \right) \quad (15)$$

here, the saturation current density, J_0 can be determined by the following equation

$$J_0 = qn_i^2 \left(\frac{D_{ni}}{L_{ni}N_A} + \frac{D_{pi}}{L_{pi}N_D} \right), \quad i=1, 2, 3 \dots \dots n \quad (16)$$

where D_{nj} and D_{pj} are the diffusion constants, and L_{nj} and L_{pj} are the diffusion lengths of the electron and hole respectively. Using the strain-dependent bandgap energy the intrinsic carrier concentration n_i can be given by

$$n_i^2 = N_C N_V \exp \left(-\frac{E_{gs}}{KT} \right) \quad (17)$$

Considering strain effect the resultant V_{oc} for a MJSC structure can be calculated by

$$V_{oc} = \sum_i^n V_{oc}(i) , i=1, 2, 3 \dots\dots\dots n \quad (18)$$

3.8 Efficiency

The efficiency of MJSC including the strain effect can be calculated by

$$\eta_i = \frac{J_{phi}V_{oc}FF}{\varphi_0} \quad (19)$$

In case of MJSC the photocurrents, J_{phi} generated in different junctions/subcells are not the same. In our calculation minimum J_{phi} is used for equalizing the photocurrents among the subcells. The efficiency is calculated considering the fill factor $FF = 0.88$ and the incident irradiance per unit area $\varphi_0 = 96.366 \text{ mW/cm}^2$ [40].

CHAPTER IV

Performance of MJSC in Presence of Strain

4.1 Introduction

In the preceding section origin of strain in MJSC structure has been discussed along with multilayer strain model. The strain-induced modification of energy bands in InGaN semiconductor has also been discussed. Furthermore, the mathematical formulations associated with solar cell efficiency in presence of strain have been explained. In this chapter, performance of different MJSC structures is determined using the formulations discussed in the previous chapter and the results obtained for different MJSC structures with and without strain effect is explained. Finally, a comparison is developed among the MJSC structures to understand MJSC structure's performance in presence of strain.

4.2 Analysis of Strain in Different MJSC structures

Using the multilayer strain model, the strain induced due to the change in lattice constants in different layers of MJSC structures is calculated. To understand the structure-dependent state of strain, equations (4) and (12) are used. Three different MJSC structures shown in figures 3.3(a-c) in chapter-3 are studied. The parameters like composition-dependent bandgap energies, lattice constants, Young's modulus, Poisson's ratio etc. are determined for InGaN by linear interpolation between the values listed in table 3.2 for the binaries GaN and InN. Initial strain plays an important role on the resultant strain, and primarily it depends on the difference of lattice constants between the substrate and bottom layer. The strain are investigated for different MJSC structures with the subcell numbers 3, 5, and 7 as a function

of subcells dimension while keeping the dimension of window, tunnel, and BSF layers are constant.

4.2.1 MJSC Structure Dependent Strain

Using the multilayered strain model, residual strain induced in different subcells of MJSC-1, MJSC-2 and MJSC-3 are estimated. The strains are calculated with respect to the MJSC subcell thicknesses. Figures 4.1(a) to (c) shows a comparison of cell position-dependent strains among the MJSC-1, MJSC-2 and MJSC-3 with the number of subcell 3. The results are calculated for the cell thicknesses 80 nm, 100nm, and 120nm and plotted in the same scale for the comparison in figures 4.1(a) to (c) respectively.

Table 4.1: Values of subcell position dependent strain with respect to subcell thickness 80 nm, 100 nm and 120 nm for different MJSC structures.

Subcell Thickness (nm)	Cell Position (nm)	Induced Strain		
		MJSC-1	MJSC-2	MJSC-3
80	150	0.0107	0.0108	0.0111
	200	0.0111	0.0113	0.0115
	270	0.0118	0.0119	0.0122
100	150	0.0104	0.0105	0.0107
	200	0.0108	0.0109	0.0112
	270	0.0112	0.0115	0.0117
120	150	0.0102	0.0103	0.0103
	200	0.0105	0.0106	0.0109
	270	0.011	0.0111	0.0114

The subcell position changes for different structures, because the number and placement of additional layers such as window, BSF and tunnel are not the same in different MJSC structures as seen in figures 3.3(a-c) in chapter 3. It is found in figure 4.1 that the magnitude of strain is the same up to the subcell position 90 nm. This is because the position of the bottom subcell and its bandgap energy is the same for all the MJSC structures up to 90 nm when subcell numbers are 3, which causes the same initial strain for all the structures.

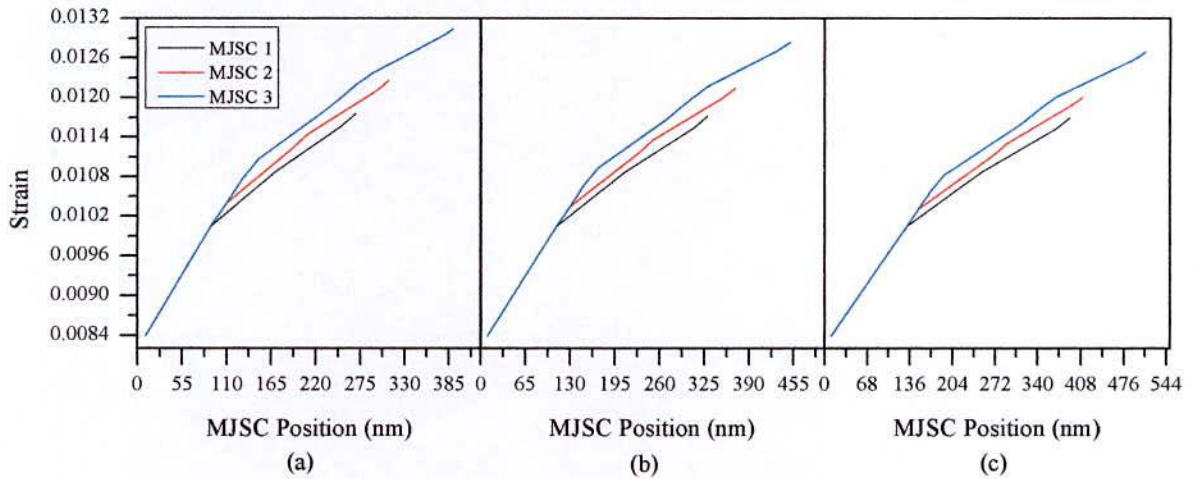


Figure 4.1: Comparison of cell position-dependent strains estimated for the MJSC-1, MJSC-2 and 3 when subcell numbers are 3 (a) 80 nm thick subcell (b) 100 nm thick subcell, and (c) 120 nm thick subcell.

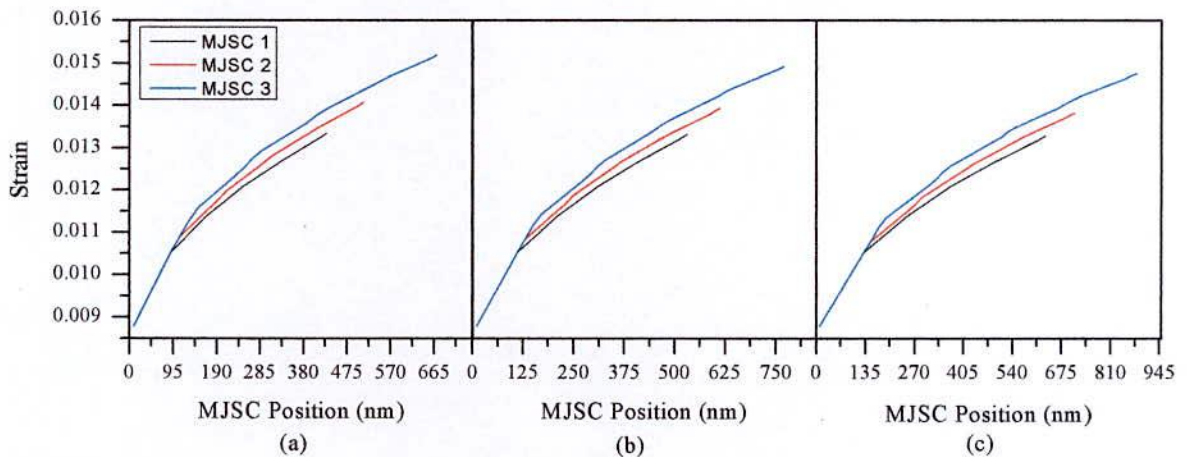
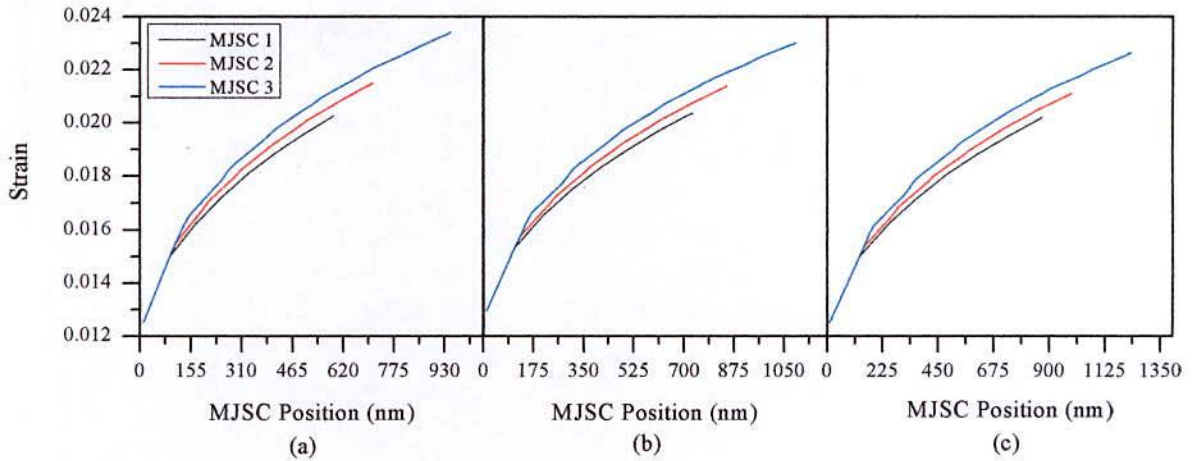


Figure 4.2: Comparison of cell position-dependent strains estimated for the MJSC-1, MJSC-2, and MJSC-3 when subcell numbers are 5 (a) 80 nm thick subcell (b) 100 nm thick subcell, and (c) 120 nm thick subcell.

After 90 nm the magnitude of the position-dependent strain varies for different MJ structures and is found to be lower, medium, and higher, for the MJSC-1, MJSC-2, and MJSC-3, respectively. This is may be due to the provision of an additional layer (tunnel) in the MJSC-2 and more additional layers in the MJSC-3. This is clearly observed in figure 3.3.



Figures 4.3: Comparison of cell position-dependent strains estimated for the MJSC structures 1, 2, and 3 when the subcell numbers are 7 (a) 80 nm thick subcell (b) 100 nm thick subcell, and (c) 120 nm thick subcell.

More number of layers in the MJSC-2, and MJSC-3 may accumulate more strain compared to the MJSC-1. Similar results are found in figures 4.2 & 4.3 for the subcells number 5 and 7. However, the magnitude of the initial strain changes for the number of subcells as the initial bandgap energies vary with the number of subcells.

In order to understand the subcell thickness dependent magnitude of strain for a particular number of subcells, figures 4.1(a) to (c) are plotted in the same scale. For the same reason, figures 4.2(a) to (c) and figures 4.3(a) to (c) are also plotted in the same scale. It is found that with increasing the thickness of the subcells from 80nm to 120nm the magnitude of the strain decreases in a particular subcell position as clearly observed in figures 4.1(a) to (c). The same results are also observed in figures 4.2(a) to (c) and 4.3(a) to (c). It is well known [35] that the strain is relaxed with increasing epitaxial layer thickness.

To compare the subcell position dependent strain with respect to different number of layer and subcell thickness the numerical values of strains are summarized in table 4.1.

4.2.2 Subcell Layer Dependent Strain

To compare the subcell position dependent strain as a function of the different layers of subcells the values of strains are estimated considering the subcell thicknesses 80nm, 100nm and 120nm subcell thickness. The strains are calculated for the MJSC-1 and summarized in table 4.2. The subcell position dependent strain profiles are plotted in figures 4.4 (a) to (c) for the layers of 3, 5 and 7. The magnitude of strain increases with the number of MJSC layers.

Table 4.2: Comparison of subcell position-dependent strain with respect to the number of subcell layers and thicknesses of MJSC-1

Subcell Thickness (nm)	Cell Position (nm)	Induced Strain		
		Layer-3	Layer -5	Layer -7
80	30	0.0088	0.0092	0.0128
	150	0.0107	0.0112	0.016
	270	0.0116	0.0123	0.0176
100	30	0.0087	0.0092	0.013
	150	0.0104	0.0109	0.0155
	270	0.0112	0.0117	0.0168
120	30	0.0085	0.009	0.0128
	150	0.0102	0.0107	0.015
	270	0.0109	0.0114	0.0164

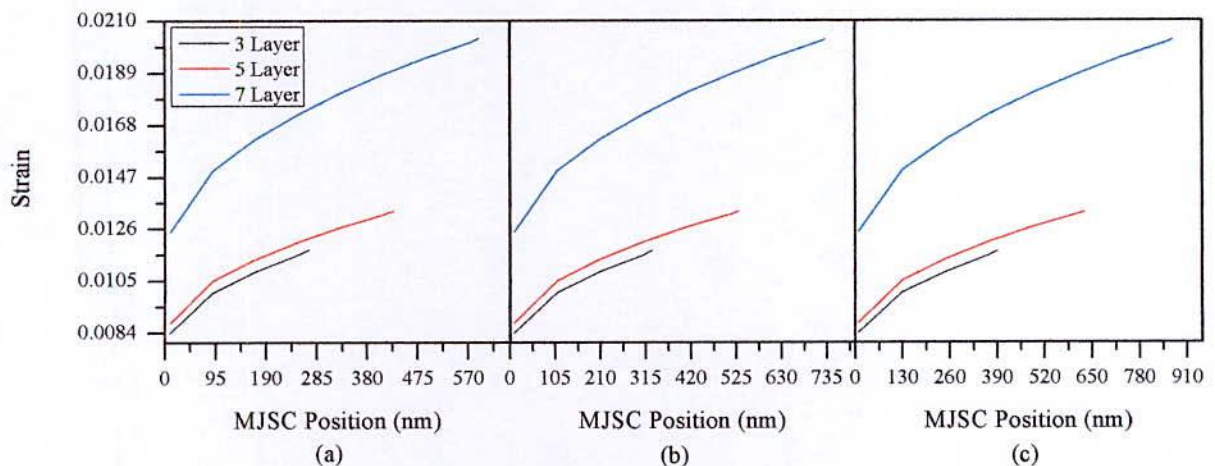


Figure 4.4 : Comparison of cell position-dependent strains estimated for the number of subcell 3, 5 and 7 of the MJSC-1 (a) 80 nm thick subcell (b) 100 nm thick subcell, and (c) 120 nm thick subcell.

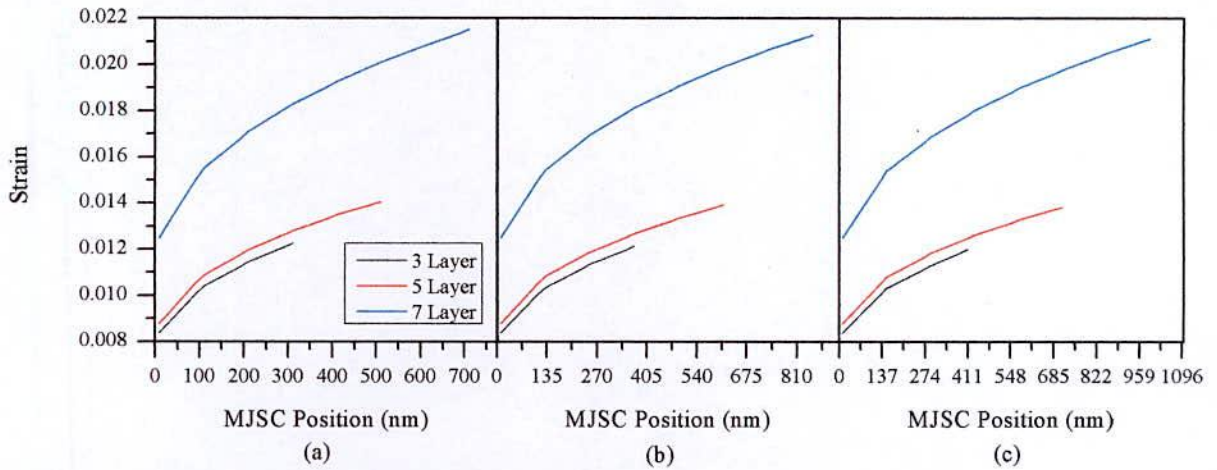


Figure 4.5: Comparison of cell position-dependent strains estimated for the number of subcell 3, 5 and 7 subcell of the MJSC-2 (a) 80 nm thick subcell (b) 100 nm thick subcell, and (c) 120 nm thick subcell.

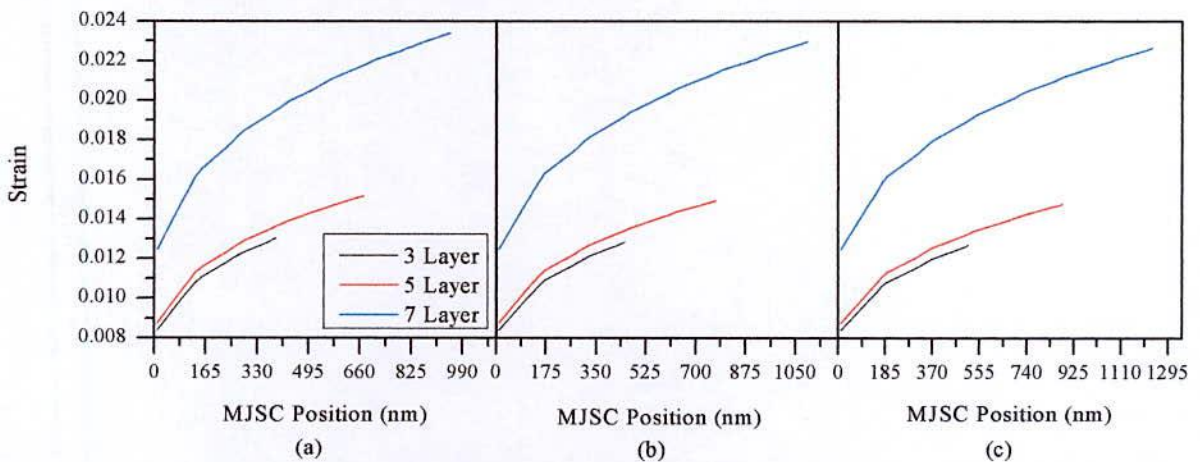


Figure 4.6 : Comparison of cell position-dependent strains estimated for the number of subcell 3, 5 and 7 subcell layered structure of MJSC-3 (a) 80 nm thick subcell (b) 100 nm thick subcell, and (c) 120 nm thick subcell

As seen in figures 4.4(a) to (c) the strain magnitude is higher for the 7 layers MJSC than the 3 and 5 layers MJSC. The strain magnitude decreases with increasing layer thickness due to the facts discussed in above. The similar results are also observed in figures 4.5(a) to (c) and 4.6(a) to (c) for the MJSC-2 and MJSC-3, respectively. However, the magnitude of strains is found to be more in case of MJSC-3 than MJSC-2 and MJSC-1, which is due to the MJSC structure as discussed earlier.

Initial strain plays an important role on the resultant strain, and primarily it depends on the difference of lattice constants (bandgap) between layer-1 and the layer below the layer-1. As seen in the above figures the value of initial strain is higher for the 7 layer MJSC and lowers for the 3 layer MJSC. This is due to the bandgap stepping for different layer of MJSC structure as seen in table 3.1.

4.2.3 Subcell Thickness Dependent Strain

To understand and hence to compare the subcell thickness dependent strains among different MJSC-structures, the values of strain with respect to the MJSC positions 90nm, 180nm and 270nm are evaluated. The results are summarized for the subcell thicknesses 80nm, 100nm and 120nm in table 4.3 considering 3-layers MJSC structures. For graphical understanding and better comparison, the strain profiles are presented in figures 4.7 (a) to (c) in the same scale for the MJSC-1, MJSC-2 and MJSC-3, respectively. It is clearly observed that with increasing the subcell thickness the value of strain decreases and same tendency is found for all the MJSC structures. The cause behind these results already discussed.

Table 4.3: Comparison of cell position-dependent strains estimated for the subcell thickness of 80nm, 100nm and 120nm when subcell numbers are 3 (a) MJSC-1, (b) MJSC-2, and (c) MJSC-3

Subcell Thickness (nm)	Cell Position (nm)	Magnitude of Strain		
		MJSC-1	MJSC-2	MJSC-3
80nm	90	0.01	0.0097	0.0095
	180	0.011	0.0106	0.0104
	270	0.0118	0.0113	0.0111
100nm	90	0.0105	0.0102	0.099
	180	0.0115	0.0111	0.01
	270	0.0122	0.0118	0.0115
120nm	90	0.015	0.0145	0.0142
	180	0.0164	0.0159	0.0155
	270	0.0175	0.0168	0.0164

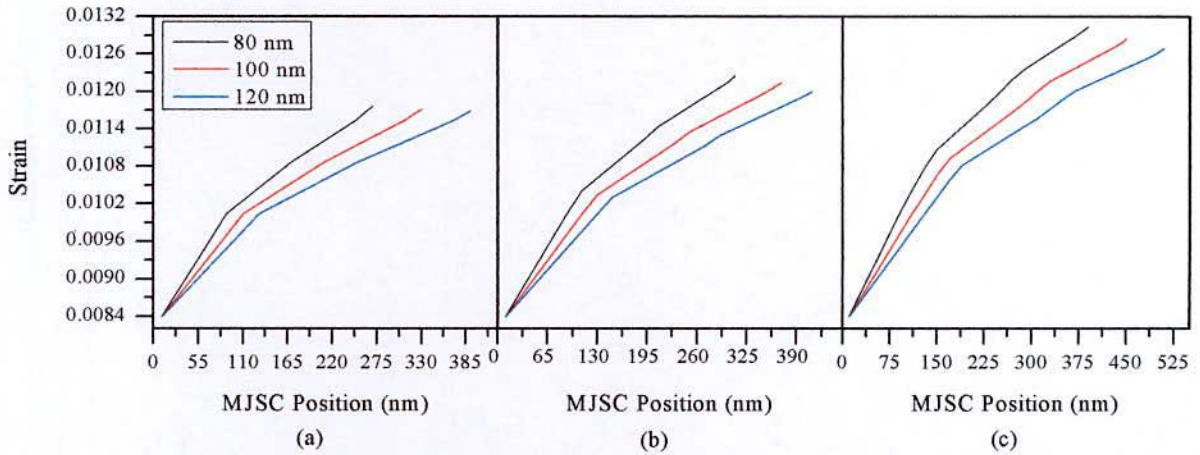


Figure 4.7: Comparison of cell position-dependent strains estimated for the subcell thicknesses of 80nm, 100nm and 120nm when subcell numbers are 3 (a) MJSC-1, (b) MJSC-2, and (c) MJSC-3.

It is also found in figures 4.7 (a) to (c) that the magnitude of strain for a particular position of subcell is more for the MJSC-3 than MJSC-2 and MJSC-1. This is due to the structural difference among the MJSCs where MJSC-3 have more additional layer than MJSC-2 and MJSC-1. The more strain for a particular position in MJSC-3 may be due to more additional layers. Similar results are also calculated and presented in figures 4.8(a) to (c) and 4.9(a) to (c) for the number of layers 5 and 7, respectively.

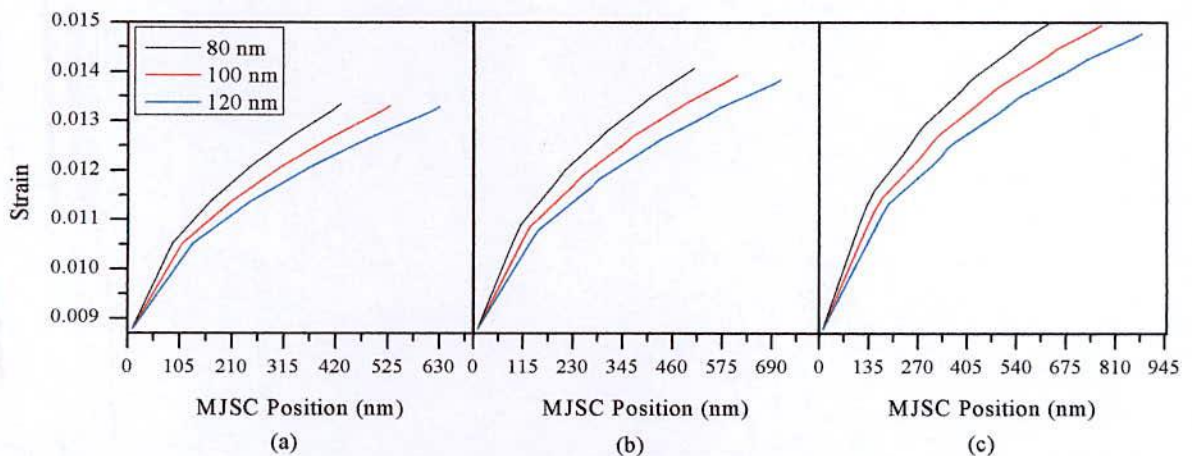


Figure 4.8: Comparison of cell position-dependent strains estimated for the subcell thickness of 80nm, 100nm and 120nm when subcell numbers are 5 (a) MJSC-1, (b) MJSC-2, and (c) MJSC-3.

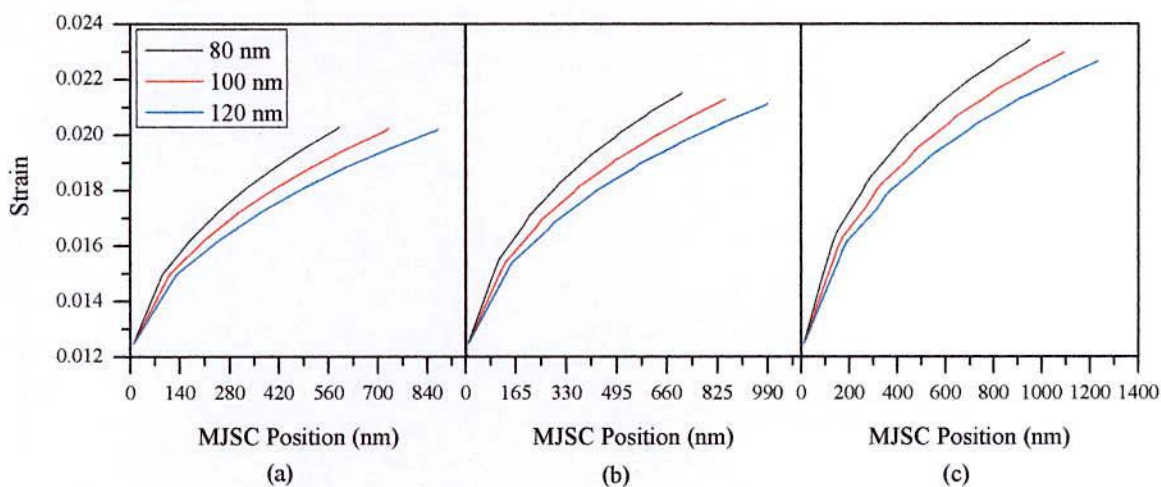


Figure 4.9: Comparison of cell position-dependent strains estimated for the subcell thickness of 80nm, 100nm and 120nm when subcell numbers are 7 (a) MJSC-1, (b) MJSC-2, and (c) MJSC-3.

4.2.4 Change in strain due to differential change in subcell thickness

The changes in strains, $\Delta\epsilon$, with respect to subcell position of different MJSC structures are determined for the number of subcell layers 3. The strains are calculated for the differential change in subcell thicknesses Δt . To calculate the $\Delta\epsilon$, subcell thickness 120nm is taken as the reference thickness and then $\Delta\epsilon$ is estimated for the differential thickness $\Delta t(120\text{nm}\sim 100\text{nm})$

Table 4.4: Change in strain, $\Delta\epsilon$, due to differential change in subcell thickness from 120 to 100nm and from 120 to 80nm

MJSC Structure	Cell Position (nm)	Change in Strain, $\Delta\epsilon$	
		$\Delta t (120-100)$	$\Delta t (120-80)$
MJSC-1	50	0.00012	0.00024
	150	0.0003	0.00054
	250	0.00038	0.00067
MJSC-2	50	0.00012	0.00028
	150	0.00026	0.00061
	250	0.0003	0.00073
MJSC-3	50	0.00012	0.00029
	150	0.0003	0.00068
	250	0.00038	0.00080

that is by subtracting the strain magnitude obtain for the thickness 100nm to that of obtained from 120nm. Similarly, the $\Delta\epsilon$ is estimated for the differential thickness $\Delta t(120\text{nm}\sim 80\text{nm})$ by subtracting the strain obtain for the 80nm subcell thickness to the 120nm thickness. The results are summarized in Table 4.4 with respect to position of different MJSC structures and plotted in figures 4.10(a) to (c) for the MJSC- to MJSC-3, respectively.

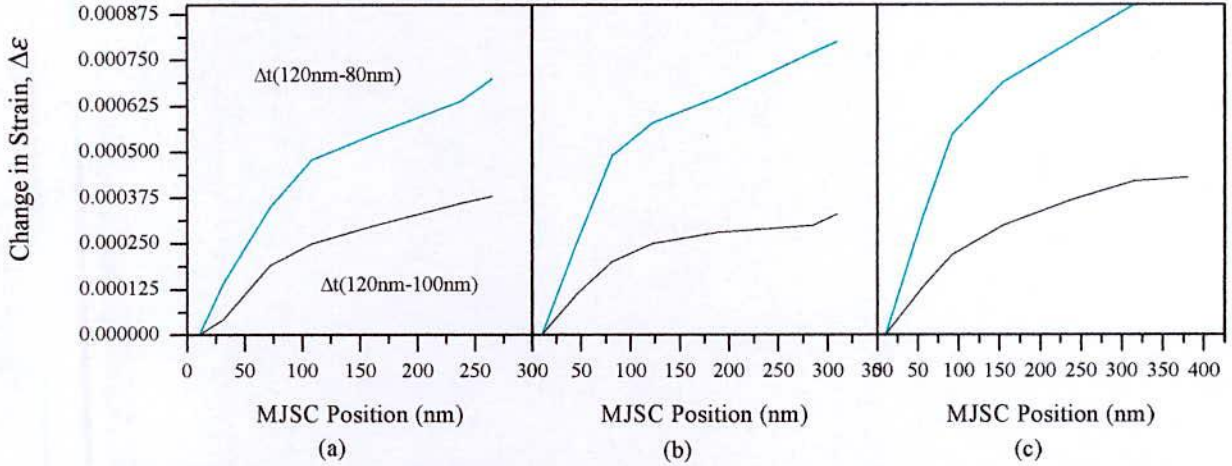


Figure 4.10: Change in cell position-dependent strains, $\Delta\epsilon$ due to the differential change in subcell thickness of $\Delta t(120\text{nm}-80\text{nm})$ and $\Delta t(120\text{nm}-100\text{nm})$ when subcell numbers are 3 (a) MJSC-1, (b) MJSC-2 and (c) MJSC-3.

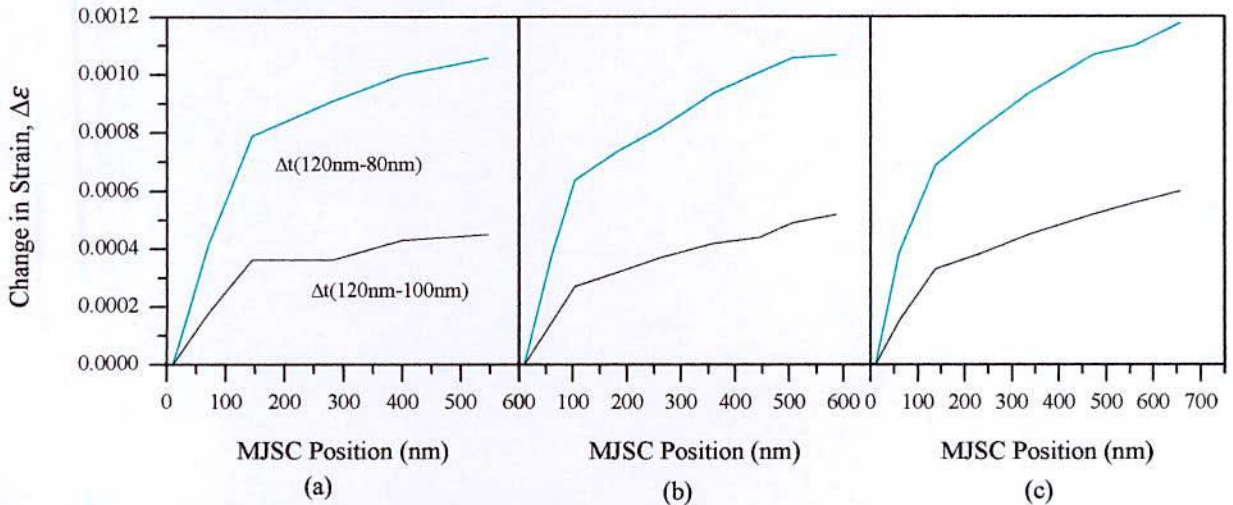


Figure 4.11: Change in cell position-dependent strains, $\Delta\epsilon$ due to the differential change in subcell thickness of $\Delta t(120\text{nm}-80\text{nm})$ and $\Delta t(120\text{nm}-100\text{nm})$ when subcell numbers are 5 (a) MJSC-1, (b) MJSC-2 and (c) for MJSC-3.

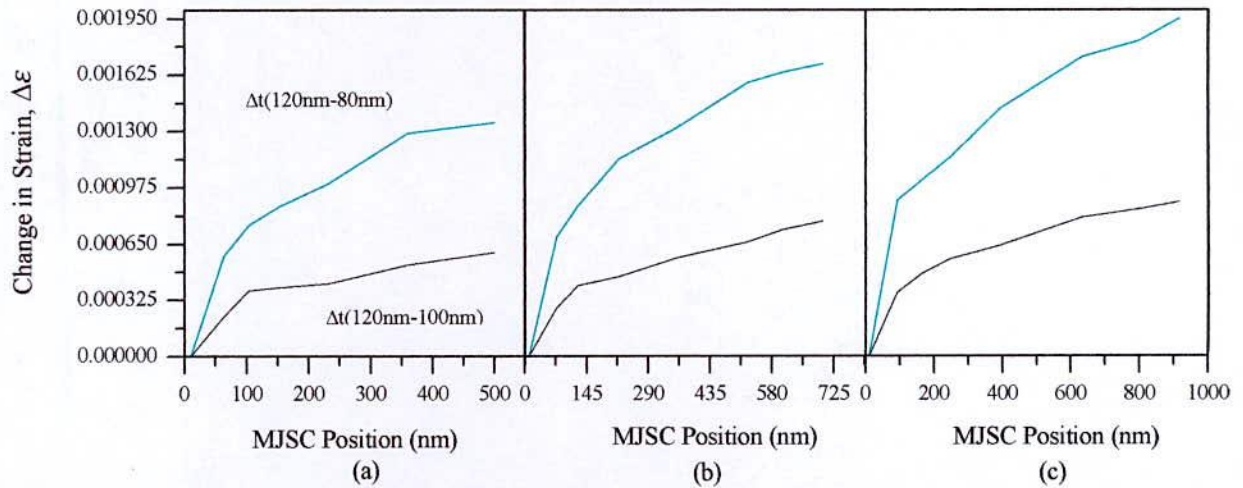


Figure 4.12: Change in cell position-dependent strains, $\Delta\epsilon$ due to the differential change in subcell thickness of Δt (120nm-80nm) and Δt (120nm-100nm) when subcell numbers are 7 (a) MJSC-1, (b) MJSC-2 and (c) MJSC-3.

It is found in figure 4.10 that the change in $\Delta\epsilon$, increases in MJSC-3 than that of MJSC-2 and MJSC-1 because, the effect of strain is more in MJSC-3 than MJSC-2 and MJSC-1 due to the provision of additional layers. Similar results are also calculated for the number of subcell layers 5 and 7 and presented in figures 4.11(a) to (c) and figures 4.12 (a) to (c), respectively for different MJSCs.

4.2.5 Strain induced change in energy gap

It is well known that the strain induced in semiconductor junction/layers due to the change in lattice constants causes a significant effect on the modification of band gap energy depending on the state of strain. Under compressive strain bandgap energy is increased in InGaN material [52]. The results are found to be opposite under tensile strain [25]. In case of MJSC studied here, tensile strain is induced in different subcell layers due to the energy stepping of the subcells and their placement in order to absorb whole solar radiations.

Table 4.5: Comparison of relaxed and strained bandgap energies under tensile strain. The results are estimated for different MJSCs having 3, 5 and 7 layers

Subcell Layers	No. of Subcell	Band Energy (eV)					
		MJSC-1		MJSC-2		MJSC-3	
		Relaxed	Strained	Relaxed	Strained	Relaxed	Strained
Layer 3	Subcell 1	0.952	0.9226	0.952	0.9226	0.952	0.9226
	Subcell 2	1.372	1.3309	1.372	1.3296	1.372	1.3274
	Subcell 3	1.899	1.8463	1.899	1.844	1.899	1.8403
Layer 5	Subcell 1	0.92	0.89	0.92	0.89	0.92	0.89
	Subcell 2	1.166	1.1272	1.166	1.1261	1.166	1.1241
	Subcell 3	1.44	1.393	1.44	1.3909	1.44	1.3876
	Subcell 4	1.757	1.7016	1.757	1.6987	1.757	1.6943
	Subcell 5	2.21	2.1448	2.21	2.1411	2.21	2.1355
Layer 7	Subcell 1	0.706	0.6741	0.706	0.6741	0.706	0.6741
	Subcell 2	0.932	0.8853	0.932	0.8838	0.932	0.8813
	Subcell 3	1.135	1.0774	1.135	1.0748	1.135	1.0705
	Subcell 4	1.355	1.2871	1.355	1.2836	1.355	1.2779
	Subcell 5	1.588	1.5105	1.588	1.5059	1.588	1.4989
	Subcell 6	1.888	1.7994	1.888	1.7941	1.888	1.7859
	Subcell 7	2.32	2.218	2.32	2.2117	2.32	2.2019

Using the deformation potentials and subcell position dependent strains, the strain induced change in bandgap energies for different MJSC structures with number of layers 3, 5 and 7 are calculated. The results obtained in our calculations are listed in table 4.5 for the cell thickness 80 nm and plotted in figures 4.13(a)-(c), 4.14(a)-(c) and 4.15(a)-(c) for MJSC-1, MJSC-2 and MJSC-3, respectively.

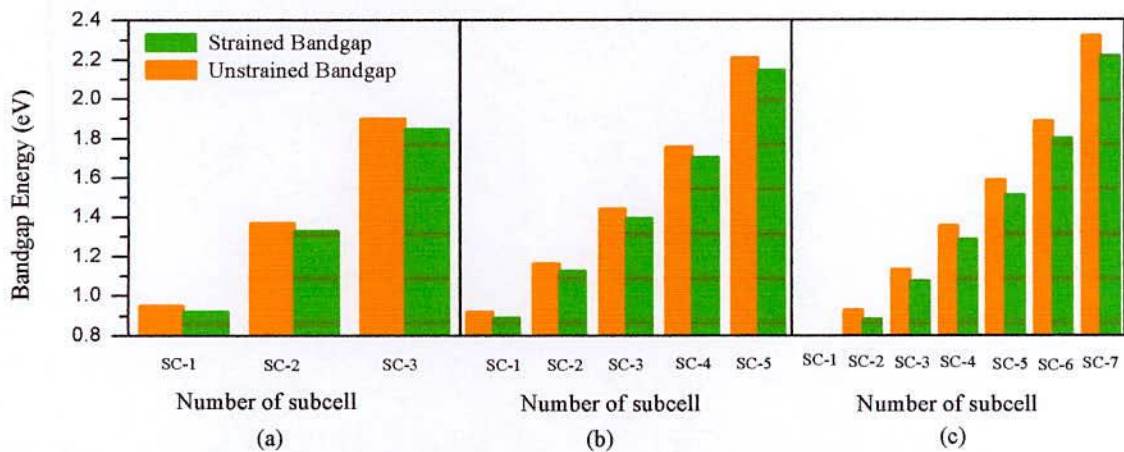


Figure 4.13: Comparison of unstrained and strained bandgap energies for MJSC-1 (a) 3-layer (b) 5-layers and (c) 7-layer with subcell thickness 80nm. The bandgap energies are estimated under tensile strained condition.

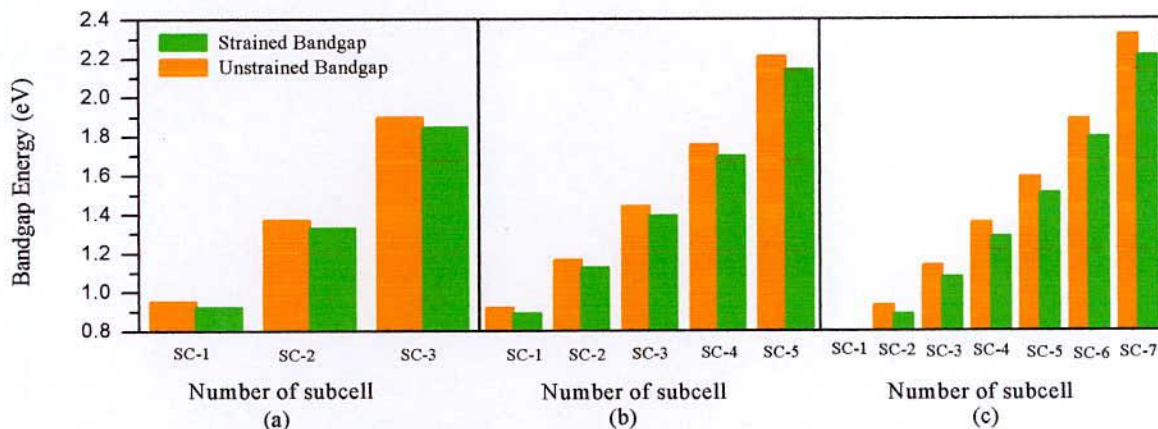


Figure 4.14: Comparison of unstrained and strained bandgap energies for MJSC-2 (a) 3-layer (b) 5-layer and (c) 7-layer with subcell thickness 80nm. The bandgap energies are estimated under tensile strained condition.

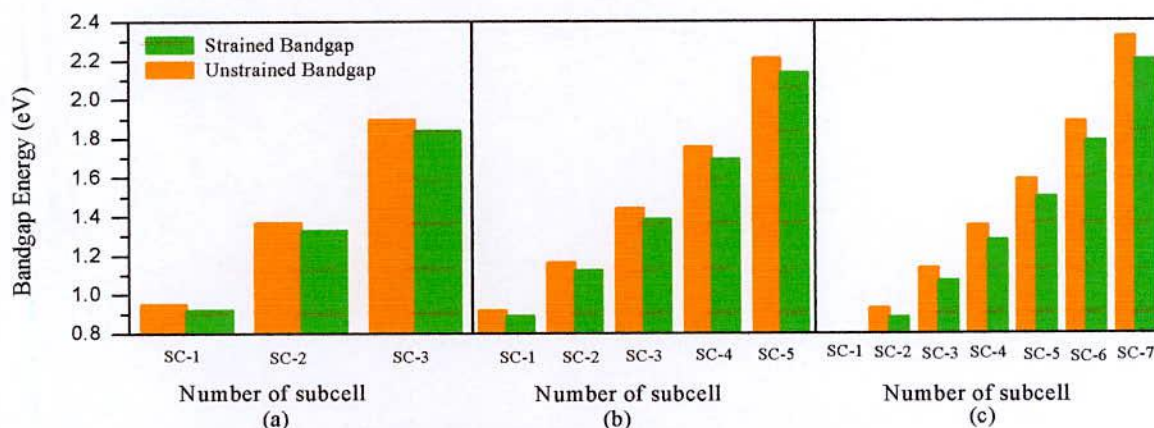


Figure 4.15: Comparison of unstrained and strained bandgap energies for MJSC-3 (a) 3-layer (b) 5-layer and (c) 7-layer with subcell thickness 80nm. The bandgap energies are estimated under tensile strained condition.

In case of 3-layer MJSC structure the bandgaps under strained condition are decreased upto 0.9226eV and 1.331eV from the relaxed bandgaps of 0.952eV and 1.372eV respectively. These reduction of bandgap energies are resulted from the position dependent strains of 0.01004 and 0.01088, respectively. In case of 5 and 7 layers, the strain dependent change in bandgap energies are also increased from the relaxed bandgap energies and found to be 1.393eV and 1.077eV from the relaxed bandgap of 1.44V and 1.135eV for the position dependent strain values of 0.01209 and 0.01725, respectively. The similar results are also

found for the MJSC-2 and MJSC-3. In all cases, the detraction of bandgap energies strongly depends on the number of layers. Even for the same MJSC structure, the decrement of bandgap energy is found to be more for the 7-layer than the 5 and 3 layers. This is due to the magnitude of tensile strain which increases with the number of layers and hence ΔE_{gs} increases. As a result, the bandgap energy under tensile strained condition obtained by equation (11) becomes reduced.

4.2.6 Change in energy gap, ΔE_{gs} , due to subcell thickness dependent strain

Using equation (10), change in energy gap due to subcell thickness dependent strain ΔE_{gs} is calculated and summarized in table 4.6. The values of ΔE_{gs} are calculated corresponding to the strain evaluated for the subcell thicknesses 80nm, 100nm and 120nm. The results are plotted in figures 4.16 (a), 4.16(b) and 4.16(c) for the number of layers 3, 5 and 7 of the MJSC-3.

Table 4.6: Comparison of subcell thickness dependent strain induced change in energy gap, ΔE_{gs} , for different thicknesses of the subcells. The comparison is made for 3, 5 and 7 layers of MJSC-3

Subcell Layers	No. of Subcell	Change in Energy Gap ΔE_g (eV)		
		80 nm Subcell	100 nm Subcell	120 nm Subcell
Layer 3	SC-1	0.02941	0.02941	0.02941
	SC-2	0.04455	0.0441	0.04376
	SC-3	0.05874	0.05795	0.05734
Layer 5	SC-1	0.02997	0.02998	0.02997
	SC-2	0.04192	0.04154	0.04119
	SC-3	0.05245	0.0518	0.05121
	SC-4	0.06275	0.06186	0.06106
	SC-5	0.07452	0.07339	0.07237
Layer 7	SC-1	0.03191	0.03189	0.03191
	SC-2	0.05072	0.0502	0.04982
	SC-3	0.06446	0.06356	0.06289
	SC-4	0.07714	0.07594	0.07508
	SC-5	0.08907	0.08759	0.08652
	SC-6	0.1021	0.10033	0.09902
	SC-7	0.11808	0.116	0.11443

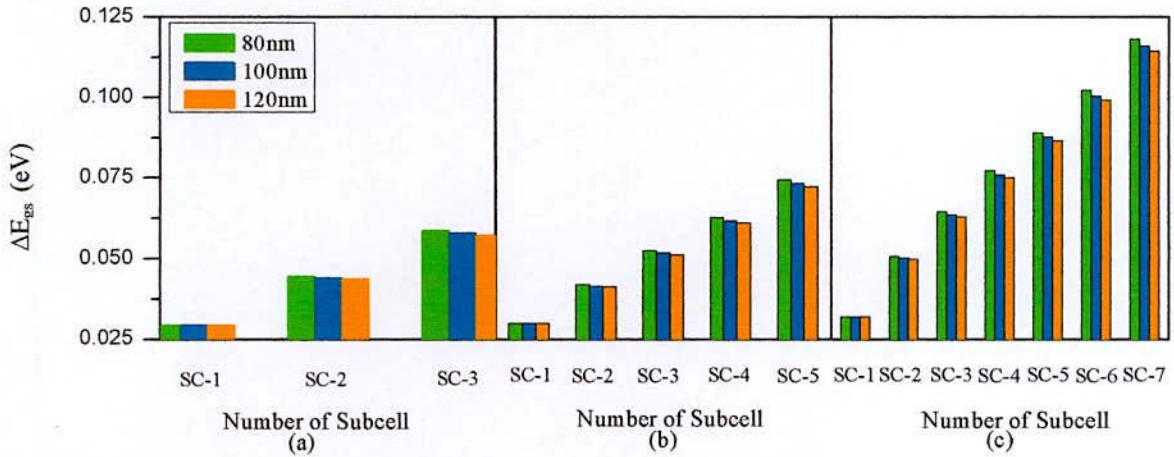


Figure 4.16: Comparison of strain-induced change in energy gap, ΔE_{gs} , for the subcell thicknesses 80nm, 100nm and 120nm. The results are estimated for MJSC-3 when the number of subcells are (a) Three (b) Five and (c) Seven.

It is found that ΔE_{gs} decreases negligibly in the bottom subcells and considerably in the top subcell for the variation of subcell thickness from 80nm to 120nm. This is because the values of strain decrease with increasing subcell thickness. The same trend is found for all the MJSC structures. The values of ΔE_{gs} for 3, 5 and 7 layers of MJSC-3 corresponding to the subcell thickness 80nm, 100nm and 120nm are summarized in table 4.6.

Table 4.7: Comparison of ΔE_{gs} for different MJSCs with 3, 5 and 7 layers

Subcell Layers	No. of Subcell	Change in Energy Gap ΔE_g (eV)		
		MJSC-1	MJSC-2	MJSC-3
Layer 3	Subcell 1	0.02942	0.02942	0.02942
	Subcell 2	0.04113	0.04241	0.04457
	Subcell 3	0.05267	0.05504	0.05873
Layer 5	Subcell 1	0.02998	0.02998	0.02998
	Subcell 2	0.03876	0.03992	0.04192
	Subcell 3	0.04703	0.04913	0.05244
	Subcell 4	0.05541	0.0583	0.06275
	Subcell 5	0.06516	0.06886	0.0745
Layer 7	Subcell 1	0.03191	0.03191	0.03191
	Subcell 2	0.04674	0.04821	0.05072
	Subcell 3	0.05762	0.06019	0.06446
	Subcell 4	0.06788	0.0714	0.07714
	Subcell 5	0.07746	0.08211	0.08907
	Subcell 6	0.08858	0.09393	0.1021
	Subcell 7	0.10196	0.10835	0.11808

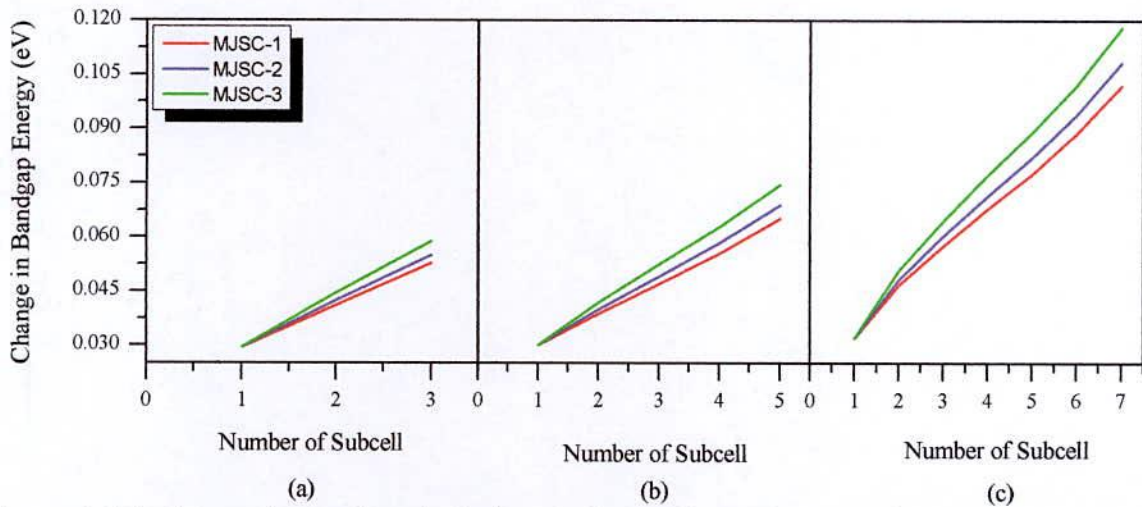


Figure 4.17: Comparison of strain-induced change in energy gap for MJSC-1, 2 and 3 structures when the numbers of subcells are (a) Three (b) Five and (c) Seven. The results are calculated for the cell thickness 80 nm.

To understand the variation of ΔE_{gs} graphically, figures 4.17(a) to (c) are plotted for different MJSCs as a function of the number of subcell layers. The values of ΔE_{gs} found to be more for the MJSC-3 than MJSC-1 and MJSC-2 and changes sharply with increasing the number of layers. The details results are summarized in table 4.7.

As discussed earlier, strain is relaxed with increasing thickness of the layer, as a result, the change in energy gap, ΔE_{gs} , due to increasing the subcell thickness decreases for all the MJSC structures.

4.3 Performance of MJSCs in presence of strain

In previous section, the MJSC structure dependent strain profiles have been presented as a function of subcell position, subcell thickness, the number of subcell layers for all of the MJSC structures. The strain-induced change in band gap energy for the InGaN-based MJSC structures and hence the bandgap energy under strained and unstrained conditions have also been shown. In this section, the effect of strain on the efficiency of InGaN-based MJSC is presented.

In order to compare the structure dependent performance of MJSC, the key parameters open circuit voltage, V_{oc} and short circuit current, I_{sc} are calculated using equation (18) and (12) for all the MJSCs under strained and unstrained conditions. Hence the efficiency η is calculated using equation (19) for the number of subcell layers 3, 5 and 7 and the subcell thickness is 100nm. Finally, the results are presented in table 4.8.

The resultant V_{oc} is determined with the summation of V_{oc} obtained from individual subcell. In this way, the value of V_{oc} for 3, 5 and 7 layer structure is determined and found to be varied from 2.45V to 5.7V in case of unstrained condition. The values of V_{oc} are found to be varied from 2.33V to 5.42V, 2.31V to 5.33V, and 2.29V to 5.12V in case of strained condition for MJSC-1, MJSC-2 and MJSC-3, respectively. These results indicate that the open circuit voltages are increased with the number of layers. MJSC-3 produces the open circuit voltage less than other structures under the strained condition. On the other hand, the current flows through a MJ solar cell from top to bottom junction is to be kept minimum. In order to equalize the photocurrent in each junction, the minimum photocurrent is taken into consideration for the calculation of MJSC efficiency.

Table 4.8: Comparison of the open circuit voltage, V_{oc} , short circuit current, I_{sc} , average number of photons and efficiency, η , for different MJSC structures with and without strain effects

No. of layer	Without strain				With strain											
	All MJSCs				MJSC-1				MJSC-2				MJSC-3			
	V_{oc} (V)	I_{sc} (mA)	Avg. no. of photon	η (%)	V_{oc} (V)	I_{sc} (mA)	Avg. no. of photon	η (%)	V_{oc} (V)	I_{sc} (mA)	Avg. no. of photon	η (%)	V_{oc} (V)	I_{sc} (mA)	Avg. no. of photon	η (%)
3	2.45	18.6	1.4628	40.18	2.33	18.8	1.3048	38.64	2.31	18.84	1.3162	38.55	2.29	18.98	1.3210	38.26
5	4.49	11.2	0.9950	44.38	4.21	11.5	0.8146	42.60	4.16	11.57	0.8157	42.46	4.08	11.69	0.8172	42.14
7	5.7	9.17	0.6871	46.14	5.42	9.38	0.7047	44.86	5.33	9.43	0.7079	44.39	5.12	9.55	0.7091	43.13

It is found in table 4.8 that the photocurrent in terms of the short circuit current I_{sc} for all the MJSC structures is varied from 18.6mA to 9.17mA under unstrained condition for the variation of layers from 3 to 7. However, the same is found to vary from 18.8mA to 9.38mA, 18.84mA to 9.43mA and 18.98 to 9.55mA for MJSC-1, MJSC-2 and MJSC-3 under strained conditions, respectively. It means that the short circuit current decreases with increasing the number of layers. This is because, the average number of integrated photons decreases under strained condition. It is found from table 4.8 that, without strain effect, the efficiencies are estimated 40.18%, 44.38%, and 46.14% for the 3, 5, and 7 layers for all the MJSCs. However, they are estimated to be 38.64%, 42.60%, and 44.86% for MJSC-1 when strain effect is taking into account. Further, if the performances of different MJSCs are compared under strained condition, the MJSC-3 shows the best results than the MJSC-1 and MJSC-2 irrespective of the layers. A comparison of efficiencies for different MJSCs is also shown in figure 4.17 under strained and unstrained conditions.

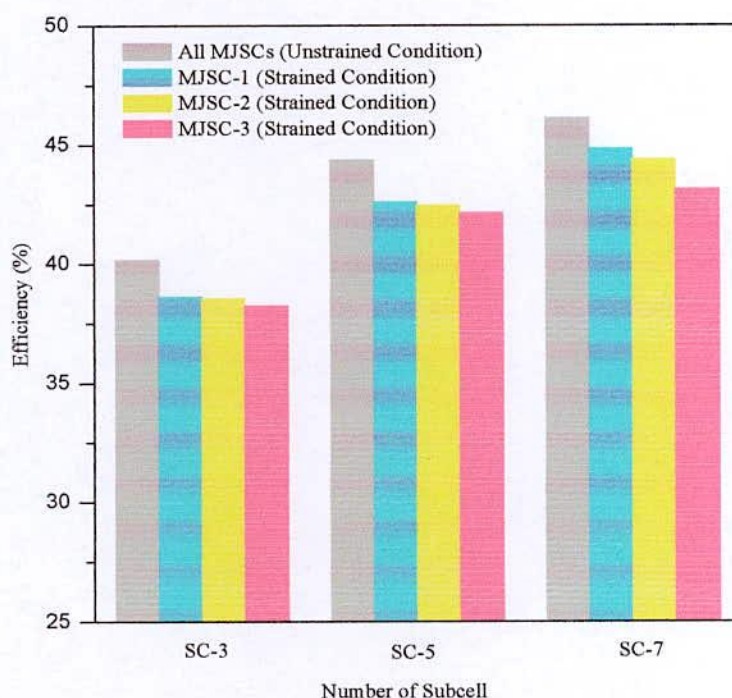


Figure 4.17: Comparison of efficiencies for different MJSCs under strained and unstrained conditions.

It is already discussed that the subcells of MJSC-3 are composed of the window layer, tunnel junction and BSF layer. The provision of more layers in the MJSC-3 causes more strain in the corresponding position of a subcell than the MJSC-1 and MJSC-2. The more strain results less open circuit voltage under tensile strain condition and hence less efficiency. The selection of subcells bandgap energies is also very much important for the MJSC structure. For the 7-layer MJSC structure, more photons are collected by integrating solar spectrum, which are happened due to suitable bandgap selection. Finally, the efficiency of the MJSC-3 for seven layer structure is found to be 43.13% which is less than the efficiencies of other structures and it reduces up to 3.01% when strain effect is taken into account.

CHAPTER V

Conclusion and Future Work

5.1 Conclusion

We for the first time investigated the residual strain, which is induced due to the change in lattice constants in different layers of InGaN-based MJSC. The effect of strain on the performance of the MJSC is also reported for the first time. We have studied three types of MJSC structures. The numbers of subcell layers are taken 3, 5 and 7 and the subcell thicknesses are taken as 80nm, 100nm and 120nm. The quantitative amount of strain is determined from the analytical approach developed for multilayered structure [24]. The results obtained from the present study demonstrate that the magnitude of strain strongly depends on the difference in lattice constant between the adjacent subcells, particularly, on the initial strain, which is induced due to the change in lattice constant between the bottom layer and the layer on which it is grown. The strain magnitude is also found to have strong dependency on the number of layers and the thickness of the subcells. The subcell position dependent strain is found to be higher for MJSC-3 than the MJSC-2 and MJSC-1. Again, the strain is found to be increased for the 7-layered MJSC structure than the 5 and 3-layered structures.

The strain-induced change in bandgap energy is determined with the combination of strain and electron-deformation potentials. The resultant bandgap energy is then determined under tensile strain condition. The results obtained in our study indicate that the open circuit voltage

of a subcell decreases under strained condition. However, the magnitudes of short circuit current are not significantly affected due to the effect of strain. With the combination of open circuit voltage and short circuit currents, the efficiencies of different MJSC structures are determined as a function of the number of subcell layers and their thicknesses. It is found from a comparison that the efficiencies for all the MJSCs is lower under strained condition than that of evaluated under unstrained condition. It is also found that thicker subcell structure gives less efficiency than thin subcell structures. Finally, it is concluded that the efficiency of the MJSC-3 for seven layer structure found to be 43.13% which is less than the efficiencies of other structures and it decreases up to 3.01% when strain effect is taken into account.

5.2 Suggestion for Future Works

In the present study, three types of MJSC structures composed of InGaN materials is investigated. The main goal of this research is to explore the influence of strain induced due to change in lattice constants in different layers of subcells. Finally, including the strain effect, the efficiency of different MJSC structures are estimated in terms of different physical parameters of the MJSC. The quantitative amount of strain is determined from the analytical approach developed for multilayered structure. The effect of series and shunt resistances has not been considered in our calculations. In future, the work can be extended considering the effect of series and shunt resistances. Using the multilayered strain model, the performance of quantum well, quantum dot, concentrator solar cell, intermediate bandgap solar cell, and multiple quantum well solar cells, can be studied in future.

References

- [1] R. Alley, "Climate Change 2007: The Physical Science Basis Summary for Policymakers," Contribution of Working Group I to the Fourth Assessment Report of the Intergovernmental Panel on Climate Change, Paris, France, Feb. 2007.
- [2] V. Panwar and T. Kaur, "Overview of Renewable Energy Resources of India," *International Journal of Advanced Research in Electrical, Electronics and Instrumentation Engineering*, vol. 3, no. 2, Feb. 2014.
- [3] M. L. Brongersma, Y. Cui and S. Fan, "Light management for photovoltaics using high-index nanostructures," *Nature Materials*, vol. 13, no. 3, Apr. 2014.
- [4] M. G. Elnugoumi, Z. A. B. Ahmed and M. Kh. M. Almsafir, "Current status and Challenges of Solar Energy in Malaysia; A Review," *Journal of Advanced Science and Engineering Research*, vol 2, no. 4, Dec. 2012.
- [5] R. S. Rohella, "Harnessing Electrical Energy through Solar Cell Concentrators," *Renewable Energy: Akshay Urja*, vol. 7, no. 1, Aug. 2013.
- [6] B. T. Gyre, "Green Energy for Green Renovation," *Geophysical Research Lett.*, vol. 36, L19704, Jul. 2012.
- [7] A. Arafath, S. Chandan and R. K. Tyagi, "Solar Tracker Mounted Battery Electric Vehicle," *International Journal of Advance Research and Innovation*, vol. 2, pp. 5-11, Sep. 2013.

- [8] A. K. Ojha, G. K. Gaur, S. Kumar and L. P. Singh, "Solar Energy and Economic Development In India: A Review," *International Journal of Emerging Technology and Advanced Engineering*, vol. 4, no. 1, Feb. 2014.
- [9] C. H. Henry, "Limiting efficiencies of ideal single and multiple energy gap terrestrial solar cells," *J. Appl. Phys.*, vol. 51, pp. 4494-4499, Aug 1980.
- [10] M. A. Green and K. Emery, "Solar cell efficiency tables (version 37)," *Progress in Photovoltaic*, vol. 19, no. 1, pp. 84-92, 2011.
- [11] T. Trupke, M. A Green, and P. Würfel, "Improving solar cell efficiencies by up-conversion of sub-band-gap light," *J. Appl. Phys.*, vol. 92, no. 7, pp. 4117-22, 2002
- [12] S. M. Bedair, M. F. Lamorte, and J. R. Hauser, "A two-junction cascade solar- cell structure," *J. Appl. Phys.*, vol. 34, no. 1, pp. 38, Jan. 1979.
- [13] J. M. Olson, S. R. Kurtz, and A. E. Kibbler, "Current matched high efficiency, multijunction monolithic solar cell," *Proc. 20th IEEE Photovoltaic Specialists Conf.*, vol. 34, pp. 257, 1988.
- [14] R. R. King, D. C. Law, K. M. Edmondson, C. M. Fetzer, G. S. Kinsey, H. Yoon, R. A. Sherif, and N. H. Karam, "40% efficient metamorphic GaInP/GaInAs/Ge multijunction solar cells," *J. Appl. Phys.* vol. 90, pp. 183516-3, May 2007.
- [15] NREL confirms world-record 43.5% efficiency on Solar Junction's CPV cell [<http://www.pv-tech.org/news>], Apr. 11, 2011.
- [16] R. K. Jones, J. H. Ermer, C. M. Fetzer, and R. R. King, "Evolution of Multijunction Solar Cell Technology for Concentrating Photovoltaics," *Jpn. J. Appl. Phys.* vol. 51, no. 10, Oct. 2012.

- [17] J. M. Olson, D. J. Friedman and S. Kurtz, "High-Efficiency III-V Multijunction Solar Cells," *Handbook of Photovoltaic Science and Engineering*, vol. 22, issue S5, pp. A1243-A1256, Aug. 2014.
- [18] H. Cotal, C. Fetzer, J. Boisvert, G. Kinsey, R. King, P. Hebert, H. Yoon, and N. Karam, "III-V multijunction solar cells for concentrating photovoltaics," *Energy Environ. Sci.*, vol. 2, pp. 174-192., Dec. 2008.
- [19] K. Tanabe, "A Review of Ultrahigh Efficiency III-V Semiconductor Compound Solar Cells: Multijunction Tandem, Lower Dimensional, Photonic Up/Down Conversion and Plasmonic Nanometallic," *Energies 2009*, vol. 2, pp. 504-530, Jul. 2009.
- [20] J. Wu, W. Walukiewicz, K. M. Yu, W. Shan, J. W. Auger III, E. E. Haller, Lu, W. J. Schaff, W. K. Metzger and S. Kurtz, "Superior radiation resistance of InGaN alloys: Full-solar-spectrum photovoltaic material system," *J. Appl. Phys.*, vol. 94, pp. 6477-6482, 2003.
- [21] A. G. Bhuiyan, A. Hashimoto, and A. Yamamoto, "Indium nitride (InN): A review on growth, characterization, and properties," *J. Appl. Phys.*, vol. 94, no. 5, pp. 2779-2808, 2003.
- [22] M. R. Islam, M. T. Hasan, A. G. Bhuiyan, M. R. Islam and A. Yamamoto, "Design and Performance of $\text{In}_x\text{Ga}_{1-x}\text{N}$ -based MJ Solar Cells," *IETECH Journal of Electrical Analysis*, vol. 2, no. 4, pp. 237-243, 2008.
- [23] X. Shen, S. Lin, F. Li, Y. Wei S. Zhong and H. Wan, J. Li, "Simulation of the InGaN-based tandem solar cells," *Proc. of SPIE*, vol. 7045, 2008.

- [24] G. P. Nikishkov, "Curvature estimation for multilayer hinged structures with initial strains," *J. Appl. Phys.*, vol. 94, no. 8, pp.5333-5336, 2003.
- [25] J. Qi and X. Qian, "Strain-Engineering of Band Gaps in Piezoelectric Boron Nitride Nanoribbons," *Nano Lett.*, vol. 12, no. 3, pp. 1224–1228, 2012.
- [26] C. G. Van de Walle, M. D. McCluskey, C.P. Master, L. T. Romano and N. M. Johnson, "Large and composition-dependent band gap bowing in $\text{In}_x\text{Ga}_{1-x}\text{N}$ alloys," *Materials Science and Engineering*, vol. 59, no. 1-3, pp. 274–278, 1999.
- [27] M. R. Islam, A. Hiroki, and M. Yamada, "Modeling and analytical calculation of strain induced by gradual variation of composition in bulk $\text{In}_x\text{Ga}_{1-x}\text{As}$ mixed crystals," *Jpn. J. Appl. Phys.*, vol. 43, no. 3, pp. 1088-1093. 2004.
- [28] Y. Nishidate and G. P. Nikishkov, "Generalized plane strain deformation of multilayer structures with initial strains," *J. Appl. Phys.*, vol. 100, no. 11, pp. 113518-4, 2006.
- [29] M. A. Rahman and M. R. Islam, "Effect of Strain on the Efficiency of InGaN-based Multijunction Solar Cell," *3rd International Conference on the Developments in Renewable Energy Technology, ICDRET 2014*, Jan. 9-11, 2014 Dhaka, Bangladesh.
- [30] <http://www.thesolarspark.co.uk/the-science/solar-power/excitonic-solarcells/dye-sensitised-cells/> on 19/08/2014
- [31] B. Burnett. The Basic Physics and Design of III-V Multijunction Solar Cells. National Renewable Energy Laboratory. Golden, CO. [Online]. Available: photochemistry.epfl.ch/EDEY/NREL.pdf, 2002.
- [32] N. Yastrebova, High-efficiency multi-junction solar cells: Current status and future potential. University of Ottawa. Ottawa, Canada. April 2007.

- [33] J. Gray, "The Physics of the Solar Cell," in Handbook of Photovoltaic Science and Engineering, Second Edition, Chichester, UK: John Wiley & Sons, 2011
- [34] B.G. Streetman and S.J. Banerjee, *Solid State Electronic Devices*, 6th ed. Upper Saddle River, Prentice Hall, ch.1-5 pp. 3-239., 2006
- [35] M. A. Green, "Solar Cell Efficiency Tables (Version 38)", *Photovolt. Res.Appl.* vol. 19, pp. 565-572, 2011
- [36] S. O. Kasap, "Principles of Electronic Materials and Devices", Tata McGraw-Hill, new Delhi, 2011.
- [37] A. G. Bhuiyan, K. Sugita, A. Hashimoto and A. Yamamoto, "InGaN Solar Cells: Present State of the Art and Important Challenges," *IEEE Journal of Photovoltaic*, vol. 2, no. 3, pp. 276-293, Jul. 2012.
- [38] S. Kolodinski, J. H. Werner, T. Wittchen, and H. J. Queisser, "Quantum efficiencies exceeding unity due to impact ionization in silicon solar cells," *Appl. Phys. Lett.*, vol. 63, no. 17, pp. 2405-7, 1993.
- [39] R. D. Schaller, V. I. Klimov, "High efficiency carrier multiplication in PbSe nanocrystals: implications for solar energy conversion," *Physical Review Letters*, vol. 92, no. 18, pp. 186601/1-4, 2004
- [40] M. R. Islam, "Design of High efficiency InGaN-based multijunction solar cell," M.Sc. Thesis paper, KUET, Khulna, Bangladesh, Nov. 2006
- [41] M. R. Islam, P. Verma, and M. Yamada, "Modeling of strain induced by compositional variation in wafer-shaped bulk mixed crystals," *Jpn. J. Appl. Phys*, vol. 43, no. 8A, pp. 5469-5476, 2004.

- [42] S. Linsel, April 2005, Technology and Future of III-V Multi-Junction Solar Cell. Georgia Institute of Technology, Atlanta [Online], Available: <http://www.stanford.edu/~slinsel/projects/solar%20report>.
- [43] A. W. Walker, O. T. Eriault, M. M. Wilkins, J. F. Wheeldon, and K. Hinzer, "Tunnel-Junction-Limited Multijunction Solar Cell Performance Over Concentration," *IEEE Journal of Quantum Electronics*, vol. 19, no. 5, Sep. 2013.
- [44] F. Bechstedt, J. Furthmüller, M. Ferhat, L. K. Tales, L. M. R. Scolfaro, J. R. Leite and V. Yu. Davydov, O. Ambacher, R. Goldhahn, "Energy gap and optical properties of InGaN," *Phys. Status. Solid.*, vol. 195, no. 3, pp. 628-663, 2003.
- [45] M. Hori, K. Kano, T. Yamaguchi, Y. Satto, T. Araki, Y. Nanishi, N. Teraguchi and A. Suzuki, "Optical Properties of InGaN with entire alloy composition on InN buffer layer grown by RF-MBE," *Phys. Status. Solid.*, vol. 234, no. 3, pp. 750-754, Oct. 2002.
- [46] X. Guo and E. F. Schubert, "Current crowding in GaN/InGaN light emitting diodes on insulating substrates," *J. Appl. Phys.*, vol. 90, no. 8, pp. 4191-4195, 2001.
- [47] Q. Yan, P. Rinke, M. Scheffler and C. G. Van de Walle, "Strain effects in group-III nitrides: Deformation potentials for AlN, GaN and InN," *Appl. Phys. Lett.*, vol. 95, no. 12, pp. 12111-1 - 12111-3, 2009.
- [48] A. F. Wright, "Elastic properties of zinc-blende and wurtzite AlN, GaN and InN," *J. Appl. Phys.*, vol. 82, no. 6, 1997.
- [49] S. M. Sze, *Physics of Semiconductor Device*, Bell Laboratories, Incorporated Murray Hill, New Jersey, 1981.

- [50] H. Salhi, H. Samet and M. Ben Amer, "Effect of BSF layer on the performance of amonocrystalline solar cell", International Renewable Energy Congress. ID 108, Nov. 2010.
- [51] C. A. Parker, J. C. Roberts, S. M. Bedair, M. J. Reed, S. X. Liu, N. A. El-Masry and L. H. Robins, "Optical band gap dependence on composition and thickness of $\text{In}_x\text{Ga}_{1-x}\text{N}$ ($0 < x < 0.25$) grown on GaN," *J. Appl. Phys.*, vol. 75, no. 17, 1999.
- [52] Oriel-Instruments. Book of Ohoton Tools, pp. 1-3, 1999.